ANYexo 2.0: A Fully Actuated Upper-Limb Exoskeleton for Manipulation and Joint-Oriented Training in All Stages of Rehabilitation

Yves Zimmermann, Michael Sommerhalder, Peter Wolf, Robert Riener, and Marco Hutter

***Abstract*—We developed an exoskeleton for neurorehabilitation that covered all relevant degrees of freedom of the human arm while providing enough range of motion, speed, strength, and haptic-rendering function for therapy of severely affected (e.g., mobilization) and mildly affected patients (e.g., strength and speed). The ANYexo 2.0, uniting these capabilities, could be the vanguard for highly versatile therapeutic robotics applicable to a broad target group and an extensive range of exercises. Thereby, the practical adoption of these devices in clinics will be fostered. The unique kinematic structure of the robot and the bio-inspired controlled shoulder coupling allowed training for most activities of daily living. We demonstrated this capability with 15 sample activities, including interaction with real objects and the own body with the robot in transparent mode. The robot's joints can reach 200%, 398%, and 354% of the speed required during activities of daily living at the shoulder, elbow, and wrist, respectively. Further, the robot can provide isometric strength training. We present a detailed analysis of the kinematic properties and propose algorithms for intuitive control implementation.**

Manuscript received 6 August 2022; accepted 28 November 2022. Date of publication 6 January 2023; date of current version 7 June 2023. This work was supported by the Swiss National Science Foundation through the National Centre of Competence in Research Robotics (NCCR Robotics). This paper was recommended for publication by Associate Editor E. De Momi and Editor E. Yoshida upon evaluation of the reviewers' comments. *(Marco Hutter and Robert Riener contributed equally to this work.) (Corresponding author: Yves Zimmermann.)*

Yves Zimmermann is with the Sensory-Motor Systems Lab, ETH Zurich, 8092 Zurich, Switzerland, and also with the Robotic Systems Lab, ETH Zurich, 8092 Zurich, Switzerland (e-mail: yveszimmer90@gmail.com).

Michael Sommerhalder and Peter Wolf are with the Sensory-Motor Systems Lab, ETH Zurich, 8092 Zurich, Switzerland (e-mail: michael.sommerhalder@hotmail.com; pwolf@ethz.ch).

Robert Riener is with the Sensory-Motor Systems Lab, ETH Zurich, 8092 Zurich, Switzerland, and also with the Spinal Cord Injury Center, Balgrist University Hospital, 8092 Zurich, Switzerland (e-mail: riener@hest.ethz.ch).

Marco Hutter is with the Robotic Systems Lab, ETH Zurich, 8092 Zurich, Switzerland (e-mail: mahutter@ethz.ch).

This paper has supplementary downloadable material available at http://ieeexplore.ieee.org, provided by the authors. The additional material provides more figures documenting the results of the experiments. The folder "ADL Trajectories" contains more visualizations of trajectories of the GH joints during ADL. The "Manipulability..." folders contain more graphics documenting the regular and directed manipulability of the shoulder. The "ROM High Resolution Grid" contains graphics describing the simulated ROM of the device in higher resolution, than the figures in the main manuscript. Links to videos documenting the experiments and the performance of the device in general are in "Video Links.pdf." The additional material contains PNG and PDF files, which can be loaded by any image viewer or PDF-reader, respectively. Contact: Yves Zimmermann - yvesz@ethz.ch for further questions about this work.

This article has supplementary material provided by the authors and color versions of one or more figures available at https://doi.org/10.1109/TRO.2022.3226890.

Digital Object Identifier 10.1109/TRO.2022.3226890

***Index Terms*—Haptics and haptic interfaces, physical human-robot interaction, prosthetics and exoskeletons, rehabilitation robotics.**

I. Introduction

WORLDWIDE, over 13.7 million people per year suffer from a stroke, and its effects [1], [2], whereby in particular elderly are at high risk for stroke. Around two-thirds of the stroke survivors lose at least partial motor control [3], [4], [5], [6]. In addition to stroke, many other diseases (e.g., Guillain-Barré-Syndrome) or traumas (e.g., traumatic brain injury) lead to similar neuromotor control deficits. However, many patients can regain some of the lost motor control [7]. Thereby, neurotherapy can remarkably stimulate the underlying recovery process (neuroplasticity) if provided at a sufficient intensity, i.e., amount of repetitions combined with the patient's high mental and physical participation. Demographic aging and the high amount of required movement repetitions [8] put pressure on health care solutions, due to an emerging shortage of qualified therapist work power to provide the required therapy.

Therapy robots have great potential to substitute the physical interaction and complement the continuous observation, online analysis, and decision making, that is, performed by the therapist during conventional therapy [9], [10]. Thereby, therapy robots may grant the therapists more time to focus on the cognitively complex aspects of therapy, e.g., observation of the therapeutic efficacy, therapy planning, and interpersonal communication. Shifting the therapist's focus more on analysis and planning of the treatment and the added functionality of the robot, e.g., quantitative analysis and high-intensity training is anticipated to improve therapy quality. Further, therapists would need less time per patient, countering the emerging therapist shortage. To maximize impact in clinical application, robots should be able to support these aspects while being applicable to provide a versatile range of neurotherapy exercises for a diverse variety of patients [11], [12], [13].

A. Performance Goals for Clinical Adoption

The robot should be able to replicate most exercise types from conventional neurotherapy [11] next to implementing novel exercise types. *Physical therapy exercises* train the general functionality of motor control, often focusing on range of motion (ROM), strength, joint coordination, and movement accuracy of single joints (joint-oriented training). *Occupational therapy*

Fig. 1. ANYexo 2.0 with a user manipulating an object.

targets the functional ability of the patient to perform activities of daily living (ADL), work, and leisure activities. Thereby, the ability to manipulate objects is in focus, while some compensatory movements might be allowed (activity-oriented training).

In addition, the robot should be able to provide these therapy forms meaningfully over the whole rehabilitation process, e.g., from severely affected to mildly affected [13]. *Severely affected patients* often cannot move the affected limb intentionally or have only little active ROM restricted to a body-proximal arm pose due to tonic spasticity. The core interest of training is to regain muscle control and extend the active and passive ROM. *Moderately to mildly affected patients* can move their arms in a relatively large ROM, can manipulate objects, and can follow more complex movement plans. The core interest of training is to enhance the strength, speed, endurance, and accuracy of hand movements and reduce compensatory movements.

Next to the above-mentioned aspects, the clinical staff considers the patient's rehabilitation stage (e.g., acute, or chronic) and personal circumstances to determine suitable therapy goals and accordingly the exercises. Further, there are many training types, which are not in the focus of the rehabilitation robot discussed here, e.g., cognitive training and speech training.

We strived to develop a therapy device [see Fig. 1] fulfilling the *Technical Feature Requirements* to effectively substitute the physical interaction between therapist and patient regarding the above-mentioned *Performance Goals for Clinical Adoption*.

II. Technical Feature Requirements

A. Robot Structure

As long as training coordination between different joints is not required for joint-oriented training, dedicated devices for each joint are the simplest solution [14]. Similarly, if coordination of a joint group like the shoulder or the wrist should be trained, dedicated robots for this group are a good match offering the least complexity and cost for the training, e.g., the OpenWrist [15]. However, kinematic and muscular synergies of the upper limb indicate the dependence of strength and ROM of a single joint on the configuration of other joints, e.g., flexion/extension synergy [16], wrist synergy [17], [18], muscle synergy [19], and task related kinematic synergies [20], [21]. Therefore, controlling the configuration of all joints with the robot while training one joint can be desired for therapy [14], [22], [23].

Rehabilitation robots that allow ADL training were presented manifold [14], [24]. To train ADL with low discrepancy to real-live tasks, the device should support 6-DOF movements of the hand. End-effector-based devices might be a good choice as the pose of the human hand is what primarily matters for the ADL execution [24]. The drawback of this architecture is that the redundancy of the human limb cannot be controlled, which leads to the training of nonphysiologic synergies. Compensatory movements and nonphysiologic synergies are often accepted in activity-oriented training of severely affected patients. However, for mildly affected patients, these synergies are mostly undesired. Further, severely affected patients require full support on all joints, as passive limb mobilization plays an essential role. Only connecting the hand to an end-effector robot would mean that all support forces are transmitted over the joints instead of the segments. This additional joint load might lead to joint irritations.

Therefore, we consider an exoskeleton architecture the best fit due to the full control over all of the limb's degrees of freedom (DOF), facilitating support for severely affected patients and correction of undesired compensatory movements. Further, for versatile joint-based and activity-based training, all DOF of the human arm should be supported by the device, particularly to allow for natural execution of activities. The human upper limb has nine relevant DOF if the manifold dexterity of the hand is not accounted for. These DOF are: sternoclavicular protraction/retraction, sternoclavicular elevation/depression, glenohumeral plane of elevation, glenohumeral elevation, glenohumeral axial rotation, elbow flexion/extension, forearm pronation/supination, wrist flexion/extension, and wrist ulnar/radial bend [25].

B. Range of Motion

Due to tonic spasticity, many severely affected patients are restricted to a body-proximal arm pose. Therapists suggest that the training should start around the center of the active ROM. Therefore, the ROM required for movements proximal to the own body (body-proximal) is essential to train those patients. Essential ADL often involve self-care, which consolidates the need for training in the body-proximal ROM. However, only a few exoskeletons have demonstrated to allow for body-proximal movements, e.g., Kim et al. [23] with restrictions of lateral adduction. Most devices, some even built for severely affected patients, have a restricted ROM for movements close to the body (i.e., restricted low humerothoracic elevation), e.g., ARMin III [26].

For joint-oriented training of mildly affected patients or orthopedics therapy, recovering the full agility of the upper limb might be a therapy goal. Hence, the robot should support the average human's active ROM.

The coupled human–robot system needs a substantial fraction of the active ROM to facilitate training of a substantial set of ADL. This ROM is only possible if glenohumeral elevation/depression and protraction/retraction are properly coordinated by kinematic design, which was partially addressed in ARMin [26], or by controlled coupling, e.g., on Harmony [27]. Other robots employ passive DOF for the glenohumeral translation [28]. However, passive DOF make parts of the robot dynamics uncontrollable, which leads to severe performance restrictions in the control of interaction forces. However, even the most advanced of these systems have limitations in the ROM and/or lack DOF restricting the training of some ADL [14], [24].

C. Training Interaction With Real Environment

Training of ADL with robots in virtual reality is well researched [29]. Therapists observed that patients struggle with the desired transfer [30] of the learned skills from robot-assisted therapy to daily living, which is supported by interpretation of results from clinical studies [9]. We suspect the lacking interaction with real objects during the training of being a relevant inhibiting factor. This statement is endorsed by studies indicating that task-oriented therapy (e.g., object manipulation) fosters faster recovery [31], [32], [33], particularly when combined with bimanual coordination [34]. Hence, the device should allow manipulation training where patients can interact with real environments, particularly including their own body.

Devices published in the state of the art put little focus on ADL training including interactions of the hand with the environment and the own body [14], [24] and exception is presented by Buccelli et al. [35]. Exoskeletons built for strength augmentation in industrial or defense applications usually have not guided the hand orientation (i.e., no wrist DOF) or did not allow direct interaction with the environment as the loads are too high for the human structure. Exoskeletons built as assistive devices, e.g., the TenoExo or the HX-β [36], [37], were designed for real-world interaction. However, these hand exoskeletons did not actively support the wrist and arm DOF.

D. Speed and Strength in High-Quality Haptic-Rendering

Moderately to mildly affected patients are usually treated with unactuated therapy devices or conventional therapy as they allow nimble and fast movements without significant resistance. For this patient group, training ADL in regular movement speeds is essential. In addition, therapy can strive to recovery of higher speeds to allow quick reactions in ADL or participation in sports, e.g., to catch a falling object. However, unactuated therapy devices (e.g., ArmeoSpring, Hocoma AG, Switzerland) cannot provide movement correction, which is usually provided by the therapist observing the therapy. Neither the assistance can be modified without therapist intervention and is often heterogeneous due to the passive support mechanism's equilibrium position (e.g., Diego, Tyromotion GmbH, Austria).

Fully actuated rehabilitation exoskeletons usually cannot render free-space (i.e., haptic transparency) for nimble movements and are typically not fast enough for moderately to mildly affected patients as they were not considered a target group so far. State of the art robots just cover velocities required in ADL, which is $3.0\,\mathrm{rad/s}$ for the shoulder and elbow as well as $8.5\,\mathrm{rad/s}$ for the wrist [38], e.g., ARMin III covers up to $3.1\,\mathrm{rad/s}$ for the shoulder joints [26]. However, these speeds are very low when compared with the capability of an unimpaired human [39], [40]. This discrepancy often leads to a feeling of being constrained by the robot, even for severely affected patients, which can cause a loss of motivation for training.

In related work, transparency was investigated for slow and smooth movements only, e.g., speeds up to $1.6\,\mathrm{rad/s}$ on ARMin IV [41]. Due to necessary control margins, high-quality transparency rendering was never possible up to the maximum speed of the actuator, which supports the demand for higher maximum actuation speeds. The first version of ANYexo achieved remarkably higher velocities of $12\,\mathrm{rad/s}$ [22] and robust free-motion rendering (i.e., high-quality transparency) was shown for dynamic movements up to $11\,\mathrm{rad/s}$ [42]. However, the ANYexo 1.0 was not equipped with wrist and forearm joints.

Achieving this robust haptic rendering of free-space is a challenge, considering that the same device should be able to mobilize a completely passive arm of a severely affected patient. Furthermore, the device should provide isometric resistance up to the average human strength to enable meaningful strength training for moderately and mildly affected patients.

E. Human–Robot Attachment

The human–robot attachment mechanism should keep the human and robot joints aligned, while transmitting forces between the human and the robot. Further, the robot should be well accessible for all patients, i.e., easy donning and doffing. Additionally, the attachment mechanism has to be efficient to use for the therapist and ergonomic for the patients [13] to achieve a high acceptance by the end-users. The robot should sufficiently support all human upper extremity segments to prevent excessive misalignment and pulling on joints. To our knowledge, other rehabilitation robots that include translation of the glenohumeral joint have not considered a solution to support the scapula or clavicle in this movement, e.g., [23]. In a recent patent, we introduced an orthosis that can support the scapula stability and mobility [43], [44]. This orthosis can be coupled with the ANYexo so that the robot guides the scapula.

For systems that do not use interaction force measurement and have high tolerances for misalignment, textile attachment systems allow a fast and toolless attachment of different arm sizes (e.g., ArmeoPower, Hocoma AG, Switzerland). However, if undesired contact points should be avoided to measure the human–robot interaction accurately, these systems are not eligible. Further, a stiff connection to the human arm facilitates transmission of interaction wrenches with high bandwidth for

haptic rendering. Robots like ARMin IV [26] have stiff connection systems that require custom padding for each user. This padding causes lowered and variable stiffness of the human–robot connection, causing inconsistency and sluggishness for haptic-rendering and higher misalignment under load. Other systems allow a stiff connection without custom components while suffering efficiency in use due to time-consuming manual adaption (e.g., Chen et al. [45]).

F. Modular Control Framework

Above-mentioned technical feature requirements indicate a high-dimensional system with powerful actuation. A method for intuitive and modular implementation of controls is required to enable the goal of providing a wide variety of exercises with such a device. Therefore, the implementation of the haptic rendering controller should be decoupled from the methods that define the haptic features to be rendered, e.g., a high-level therapy control methods (HTCA), online collision avoidance, and patient specific constraints. Thereby, the high-level methods are decoupled from each other, which allows modular recombination and independent method modification. For therapy devices, controllers are mostly developed in an integrated way for a specific exercise causing low flexibility in altering and recombining methods. A more distributed and modular approach is standard in other robot applications, e.g., in mobile autonomous robots.

Training ADL in close proximity of the own body introduces the risk of undesired collisions. Hence, the robotic system should know the location of the user's body surface. Body-proximal movements were not in the core focus of exoskeletons powerful enough for full support or even strength training. However, concepts to improve the safety of robots operating in the proximity of a human body in general were presented, e.g., series elastic actuation (SEA) [46] and lightweight design. In a recent publication, we introduced a method to track the head and torso surface of the user to avoid collisions during body-proximal training enabling such movements with ANYexo [47].

G. Requirement Summary

Following technical feature requirements should be considered during the development process.

Robot Structure (R-A): We considered an exoskeleton robot structure covering all nine relevant DOF of the human arm to be the best fit to fulfill the *performance goals for clinical adoption*. So far, no exoskeleton has been presented that would cover all relevant DOF while providing sufficient actuation power to provide support in therapy.

ROM (R-B): We strive for covering the full active ROM of the human [see Fig. 7(b)], particularly including body-proximal movements, while considering human joint synergies. The scientific challenge is to find a kinematic structure that fits around the human upper limb and achieves this ROM incorporating all relevant DOF. To allow for the execution of all relevant ADL, a smaller ROM might be sufficient [see Fig. 9].

Training Interaction with Real Environment (R-C): We strive to augment the state of the art by combining the ability to interact with the environment and the own body with a fully actuated exoskeleton including the wrist. Here, the challenge is to design the kinematic structure and links such that collisions with the environment and the own body are prevented while allowing interaction with the same.

Speed and Strength in High Quality Haptic-Rendering (R-D): The robot should support speeds significantly higher than the ones required for ADL and be capable of establishing interaction torques large enough for maximum isometric strength training of average humans. Quantitative values can be found in Table III. The challenge is to find the right tradeoff between actuation power, inertia, and ROM of the robot (reduced by bulky actuators).

Human–Robot Attachment (R-E): The full kinematic chain of the human upper limb should be well positioned and supported by the human–robot attachment concept while keeping the operation of the attachment mechanisms time efficient. The challenge is to design the attachment concept with a slim design facilitating a large ROM while incorporating the required functionality.

Modular Control Framework (R-F): The complexity of the control framework should be broken down and the implementation should be flexible, to allow efficient development of versatile therapy exercises. Therefore, the submethods of high-level therapy controls, haptic rendering, and safety algorithms should be implemented in a modular way using the space representation that is most intuitive. Algorithms independent of these modules should be used to coordinate and merge the single modules' contribution into the system's holistic behavior.

H. Limitations of the State of the Art

No device known to the authors combines all of these *Technical Feature Requirements* that are needed to maximize the impact of upper-limb therapy robots by facilitating the *Performance Goals for Clinical Adoption*.

A selection of representative state-of-the-art fully-actuated upper limb exoskeletons are ANYexo 1.0 [22], ARMin [26], and Harmony [23]. The ANYexo 1.0 did not include any wrist DOF and therefore was highly limited for training ADL. ARMin and Harmony did better in this regard, as both included two DOF in the wrist. However, for full dexterity a three DOF wrist is required. ARMin and particularly Harmony were restricted to slow training speeds according to published data and available videos. ANYexo 1.0 provided only 39 Nm of torque on the shoulder joints, which strongly restricted the forces it could act on users. ARMin had strong restrictions for body-proximal movements due to rather bulky design of the internal/external rotation mechanism and did not include sternoclavicular joints, which are necessary to reach the far parts of the human's ROM. Harmony had less restrictions in body-proximal movements than ARMin. However, for Harmony restrictions of body-proximal movements in the frontal plane existed and the nonorthogonal angles of the GH-joint reduced the manipulability of the kinematic structure.

A device fulfilling these requirements would have the advantage that therapists and patients only need to learn one system [11]. Individual patient parameters could be adapted continuously, and transfer of individualization is possible over

multiple stages of therapy. Versatile applicability for many exercises and patients would make it easier to keep the occupancy rate of the device high. Here, we described the design of the upper-limb rehabilitation exoskeleton ANYexo 2.0 and analyzed its performance. This robotic system achieved sufficient ROM, manipulability, speed, and strength to provide meaningful physical and occupational therapy for severely to mildly affected patients regarding the physical interaction aspect. The other aspects needed for a complete therapy device, e.g., continuous observation, online analysis, and decision making, were or will be addressed in other works, e.g., [47].

III. System Description

The design of the ANYexo 2.0 uses the same kinematic structure for the shoulder joints as presented by Zimmermann et al. [22] for the first version of the robot. Motivated by the technical feature requirements, an active controlled bio-inspired coupling for the shoulder was implemented (R-B/E), a fully actuated wrist module was developed (R-A/E), the actuator choice was optimized (R-D), the attachment system was revised (R-E), and methods to facilitate modular and intuitive control were developed (R-F).

A. Kinematic Structure

The robot should incorporate all nine relevant DOF of the human arm. These DOF can be summarized into four groups: a 2-DOF sternoclavicular joint (SC), a 3-DOF glenohumeral joint (GH), a 1-DOF elbow (EB), and a 3-DOF wrist (WR). The human SC joint is complex with many individual DOF of the clavicle and the scapula. Most of these DOF can either be lumped with the rotational DOF of the GH joint or have a negligible ROM. The relevant SC-DOF are shoulder protraction/retraction (GPR) and elevation/depression (GED), which were implemented with perpendicular and intersecting axes on the robot. The humeral head translates w.r.t. the glenoid socket. However, this translation can either be lumped with the two SC-DOF or have a negligible ROM. Hence, the GH joint was approximated by a spherical joint (GH robot joints: GHA, GHB, and GHC). The elbow was approximated as a hinge joint for the flexion/extension movement (EFE). The kinematic structure of the human wrist is a complex interplay of eight bones. The relevant human wrist DOF are flexion/extension (WFE) and ulnar/radial deviation (WUR). The main rotation axes of the human wrist for extension, flexion, radial deviation, and ulnar deviation do not intersect, according to Neu et al. [48]. However, the minimum distance between these axes was assumed lower than 4 mm. Hence, the wrist joint can be simplified to a single WFE and a single WUR axis that are perpendicular and intersect by accepting little misalignment. The human forearm pronation/supination (WPS) was simplified to a rotation axis intersecting the elbow and wrist axes. Thereby, the forearm and wrist DOF were summarized to a spherical joint WR at the wrist with the robot joints: WRA, WRB, and WRC [see Fig. 2(b)].

The kinematic structure for the six proximal DOF is identical to the kinematic structure presented in [22]. For the development of the wrist's kinematic structure [see Fig. 2], following aspects were considered. The axes should be oriented as close to orthogonal as possible in the center of the ROM to achieve the best manipulability, which would benefit the available robot speed in any direction (R-D). Collisions of the wrist components with human and other robot components should be avoided to achieve the biggest possible ROM for the wrist and the least restriction of the proximal exoskeleton components (R-B). For collisions with the human, particularly body-proximal movements were considered. The human–robot attachment should be accessible without moving the hand through a confined space for easy access by severely affected patients (R-E).

To evaluate collisions during the development process, collision boxes were attached to the CAD of the exoskeleton for all critical configurations resulting in a summary visualization of the restrictions for the footprint of the wrist components [see Fig. 3].

We compared parallel kinematic concepts [23], [49] and series kinematic concepts [15], [26], [50] regarding our goals and available actuators. The solution with the best overall performance regarding our goals was a series kinematic design due to the lightweight and lower footprint design with the same stiffness and ROM. Direct actuated joints, where the actuator and joint bearing can be in one unit and minimal transmission elements are needed, were selected due to lower the footprint, see in Fig. 2(b). For an improved ROM by self-collision avoidance, a nonorthogonal angle between the first two wrist axes was accepted. For this kinematic concept, the EFE actuator was moved while the shoulder's kinematic structure remained the same as for ANYexo 1.0 presented by Zimmermann et al. [22]. Interactions with the own body were promoted by placing the most distal actuator at the ulnar side of the wrist. However, e.g., manipulating objects on a table would be restricted due to collisions of the actuator with the table. To prevent collisions during such ADL with real environments, the WRC actuator could be swapped to the radial side ("alternate kinematic structure of the wrist").

Singularities in the spherical GH and WR joint were prevented by choosing the position of the mechanical end stops of the GHB and WRB joints such that singular positions could not be reached. As the WRB joint almost coincides with the direction of ulnar/radial deviation, in which humans have a small active ROM, the placement of the mechanical end stops does not limit the relevant operational ROM of the robot.

B. Links

The development of the links focused on lightweight design, stiffness, low inertia, collision avoidance, and preventing pinching hazards (R-A...D). The mass from links and actuators were placed as close to the rotation axes as possible to keep the inertia low as only a fraction of the inertia can be compensated when rendering interaction forces [42]. The links were designed with milled aluminum parts connected with glued stock carbon fiber reinforced plastic (CFRP) tubes [see Fig. 4]. The hollow CFRP tubes were used for cable guidance where possible. All joints were built with mechanical end stops to prevent overextension. 3D-printed PA-12 covers mitigated the pinching hazard at the joint end-stops. We chose the location of the actuators and the

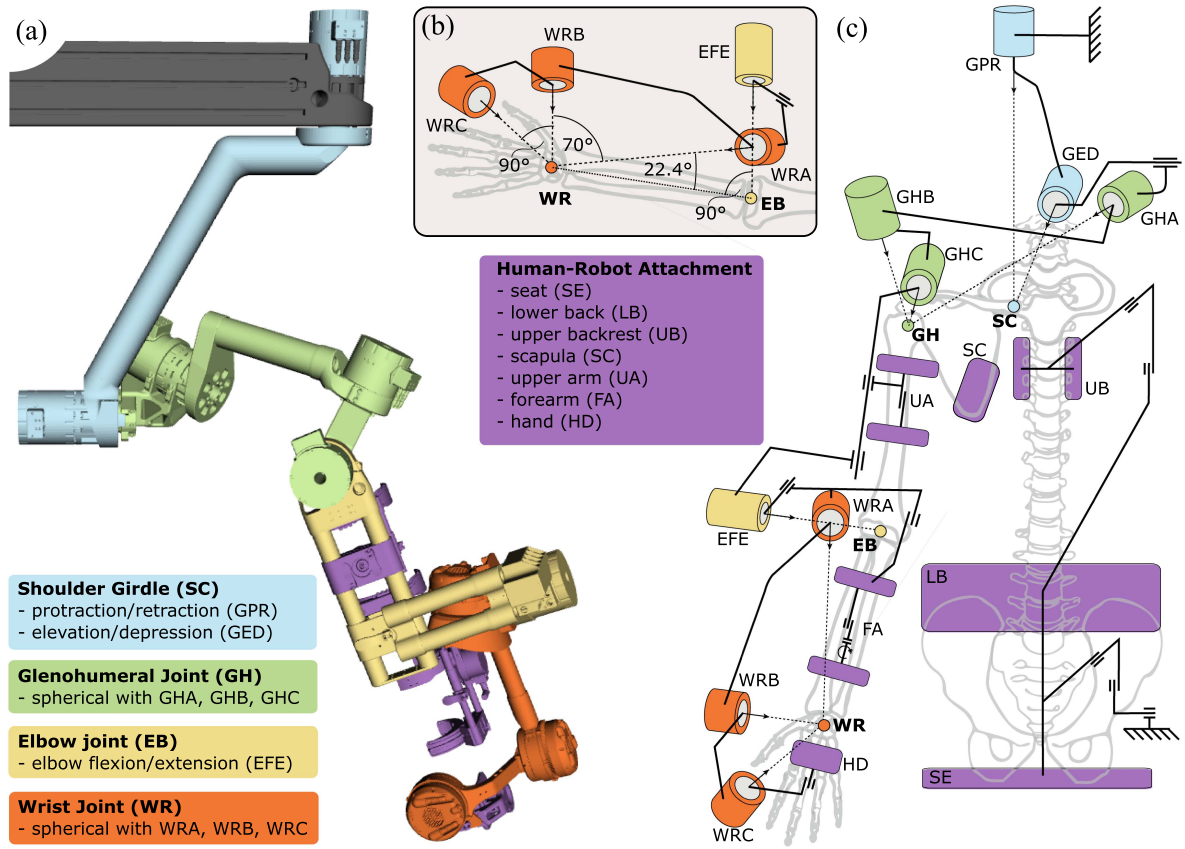

Fig. 2. Kinematic structure of the ANYexo 2.0 including the human–robot attachment points. The color-coding highlights the functional groups of the rendered parts and kinematic components according to the legends in the graphic. (a) The colored rendering of the ANYexo 2.0 arm with the standard configuration of the wrist. Most of the base structure (gray) and the torso attachment are clipped. (b) Closeup of the wrist's kinematic structure with the geometry resulting out of the design process. The WRB actuator lies on the ulnar side of the wrist in "standard" configuration. (c) The kinematic tree with actuators, prismatic joints for length adaption, and human–robot attachment including the torso constraints.

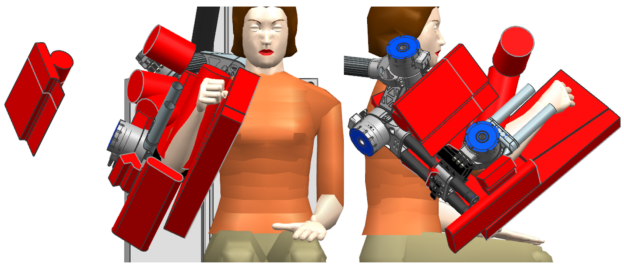

Fig. 3. Red geometrical shapes mark the space, where parts of the wrist module should not be located to avoid collisions with the proximal exoskeleton components and the user's body.

shape of the wrist module's links such that collisions with the user's body and other robot components do not occur in an as large as possible ROM. Therefore, we used the same summary visualization of restricted build space as for the kinematic structure [see Fig. 3].

C. Human–Robot Attachment

The torso was positioned by a chair with a seat, a lower backrest to define the pose of the hip, and an upper backrest to prevent undesired compensation movements or slumping of the upper torso during training. At the upper arm and forearm, we implemented two contact points at each segment's proximal and distal end to achieve a high stiffness of the overall connection and distribute the interaction forces acting on the arm. The attachment mechanisms were designed with nonflexible components such that a stiff connection was established [see Fig. 4]. Only 2.5-mm neoprene cushioning was used. Arms of different diameters were automatically placed at the same distance w.r.t. the exoskeleton by tightening and fixing the attachment mechanism (patent pending EP21205583.4). The hand attachment mechanism for manipulation training consisted of a plate that contacts the metacarpals of the hand on the dorsal side. A 25-mm-wide textile strap with Velcro over the palmar side fixed the hand to the plate while allowing to grasp objects. For training where grasping was not necessary, a simple cylindrical grip was also available.

D. Adaptability to User's Size

The robot was built adaptable for the fifth percentile female to 95th percentile male by fixed passive prismatic joints [see Fig. 2]. The arm length geometry could be adapted by three joints for the clavicle, upper arm, forearm length. The human–robot attachment system involved five joints in the chair and upper

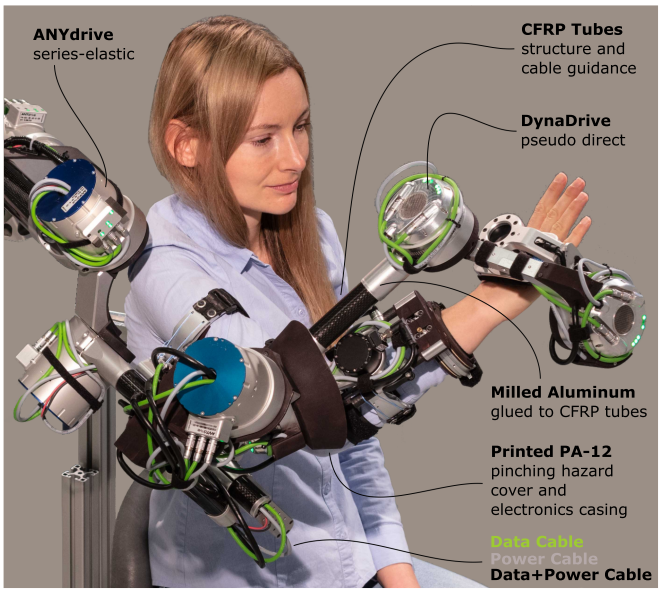

Fig. 4. Closeup of the exoskeleton arm with user.

backrest, two joints for the upper arm and forearm cuff positions each, and one joint simultaneously adapting hand length and width. The attachment system automatically adapted to the arm circumference of the upper arm and proximal forearm when fastening (as shown in patent application EP21205583.4). Adapting the robot thoroughly to a new user took around 10 to 15 min. The settings were repeatable within around 2 min, making the reattachment efficient and accurate.

E. Actuation and Instrumentation

All joints should provide precise and robust torque control and facilitate maximum speeds that results in faster movements than used during ADL. Further, the actuators should provide a maximum joint torque that allows at least moving the passive arm of a 95th percentile male (R-D). Further, aiming to provide maximum strength training up to the average population performance was desired (the quantitative requirements are stated in Section VI alongside the results). To achieve robust torque control performance, we considered only direct, quasi-direct, and series-elastic electric actuation (SEA). Pneumatic actuation was not an option as a torque control bandwidth significantly higher than the human torque control bandwidth (5 to 10 Hz [51]) was required for sufficient haptic-rendering performance [28].

Due to the high torque requirement for the shoulder joints SC and GH, caused by the weight of the robot's wrist and human arm, we decided on the SEA actuators ANYdrive 2.0 with a 1:100 gear ratio (ANYbotics AG, Switzerland). Due to the lower torque requirement, we chose an ANYdrive 2.0 with a 1:50 gear ratio for the elbow. For the wrist, the required speeds were higher and the torques lower. Therefore, we implemented the quasi-direct drive Dynadrive Armadillo (Robotic Systems Lab, Switzerland), see Table I. All drives have a torque control bandwidth up to 60 Hz for small amplitudes.

TABLE I
ACTUATOR SPECIFICATIONS: $\dot{q}_{MAX}$ IS THE MAXIMUM SPEED, τ_{MAX} THE PEAK TORQUE, P_{NOM} THE NOMINAL POWER, AND P_{MAX} THE PEAK POWER

actuator type	weight (kg)	$\dot{q}_{max}$ (rad s^{-1})	τ_{max} (N m)	P_{nom} (W)	P_{max} (W)
ANYdrive (1:100)	1.4	6	77	240	720
ANYdrive (1:50)	1.1	12	39	240	720
Dynadrive	0.8	30	23	200	320

All actuators had integrated joint bearings, an onboard motor controller, joint encoders, IMU, and EtherCAT communication unit. The three human–robot interaction points at the upper arm, the forearm, and the hand were each equipped with a 6-DoF force-torque sensor Rokubi Mini (Bota Systems AG, Switzerland) with integrated IMU, acquisition boards, and EtherCAT communication. The integrated electronics in all actuators and sensors avoid electromagnetic interference on the robot and reduce cabling. The standard sampling and control rate for the control PC (Ubuntu 20.01) was 800 Hz while the torque, position, and velocity controllers on the drives ran with 4 kHz.

F. Definition of Coordinate Systems

Here, we introduce two joint-based coordinate systems that we used to control the ANYexo. Both are minimum coordinates to describe the state of the device. The exoskeleton joint coordinates (EXO) coincide with the rotation joints of the robot. Hence, EXO describes the joint state of the robot [see Fig. 2]. The EXO coordinates are very specific to the robot's kinematic and not particularly intuitive to understand for clinical staff. Therefore, we defined the clinical joint coordinates (CJC) based on the suggestions of Wu et al. [25]. The translation of the GH joint was described by shoulder protraction/retraction (GPR) and shoulder elevation/depression (GED). The orientation of the humerus w.r.t. the torso was described by a serial kinematic spherical joint with DOF plane of elevation (POE), angle of elevation (AOE), and internal/external rotation (IER) [see Fig. 5(a)]. Hence, differently from the EXO coordinates, the CJC described the pose of the upper arm not as a pure serial kinematic structure [see Fig. 5(b)]. The GED joint and GPR joint DOF of the EXO coordinate system and the CJC were identical. The same applied to the elbow flexion/extension (EFE) joint. For the wrist, the CJC used the commonly known DOF pronation/supination (WPS), wrist flexion/extension (WFE), and ulnar/radial bend (WUR) in a series kinematic configuration. Differently from the EXO coordinate system, consecutive joint axes of the CJC wrist were all perpendicular to each other. Even though the WRB joint almost matched the WUR, these DoF were not the same. As WUR required the smallest ROM for ADL [52], we defined it as the last DOF of the CJC, while WRB was the second last joint of the EXO.

G. Coordinate Conversions

Optimization methods such as hierarchical quadratic programming and trajectory optimization require, differentiable conversions of positions θ, velocities $\dot{\theta}$, and accelerations $\ddot{\theta}$ between the reference coordinate systems. We are looking for

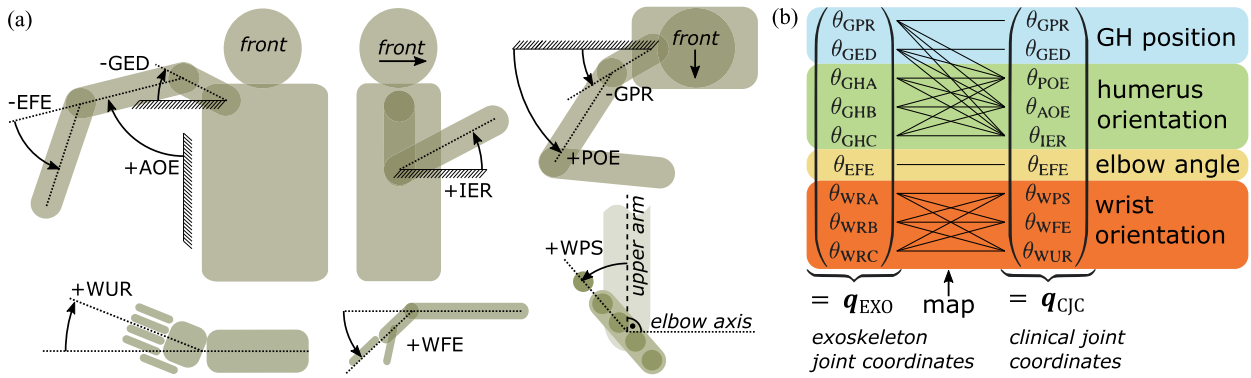

Fig. 5. Clinical Joint Coordinates (CJC). (a) Definition of sign and zero position of the CJC: shoulder elevation(−)/depression(+) (GED), plane of elevation (POE), angle of elevation (AOE), internal(−)/external(+) shoulder rotation (IER), elbow flexion(−)/extension(+) (EFE), wrist pronation(−)/supination(+) (WPS), wrist flexion(+)/extension(−) (WFE), wrist ulnar(+)/radial(−) bend (WUR). (b) Mapping of CJC to exoskeleton joint coordinates (EXO) [see Fig. 2].

analytic linear conversions for velocities and accelerations to use efficient optimization algorithms. Conversions between the robot joint coordinate system (EXO) and the hand position in the world frame (HND: task space) are a standard in robotics and do not need further explanation. On the contrary, the conversion between the CJC and the EXO coordinates is specific to the application. Our proposed CJC for the upper limb contains partially parallel kinematic structures in the shoulder. Thus, common Jacobian derivation methods cannot be applied. Here, we introduce a method to compute the Jacobians relating velocities and accelerations between the proposed CJC and any robotic joint coordinates with the example of the EXO coordinates. The GPR, GED, and EFE movements are identically defined for CJC and EXO [see Fig. 5(b)]. Hence,

$$\theta_i^{\mathrm{EXO}} = \theta_i^{\mathrm{CJC}}, \quad \dot{\theta}_i^{\mathrm{EXO}} = \dot{\theta}_i^{\mathrm{CJC}}, \quad \ddot{\theta}_i^{\mathrm{EXO}} = \ddot{\theta}_i^{\mathrm{CJC}} \tag{1}$$

for $i \in \{\mathrm{GPR,GED,EFE}\}$. The torque conversion for GPR and GED is not straightforward as $\tau_{\mathrm{GPR}}^{\mathrm{CJC}}$ and $\tau_{\mathrm{GED}}^{\mathrm{CJC}}$ depend on the torque of the humeral orientation degrees (POE/AOE/IER) due to the parallel structure [see Fig. 5]. The torque conversion for the elbow is trivial

$$\tau_{\mathrm{EFE}}^{\mathrm{EXO}} = \tau_{\mathrm{EFE}}^{\mathrm{CJC}}. \tag{2}$$

The equations for the conversion for positions and Jacobians for the conversion of velocities, accelerations, and torques between the EXO and CJC system are described in Appendix A. Further, the Jacobian describing the coupled shoulder rotational velocity in CJC coordinates $\tilde{\mathbf{J}}_{\mathrm{CE}}^{\mathrm{coup}}$ and WRD coordinates $\mathbf{J}_{\mathrm{r,H}}^{\mathrm{EXO,coup}}$ w.r.t. the GH rotation expressed in EXO coordinates can be found as well in Appendix A.

IV. Controls

A. Active Shoulder Synergy

The human shoulder achieves its large ROM through the sternoclavicular, scapulothoracic, acromioclavicular, and glenohumeral joint synergy. The shoulder muscles and ligaments control this synergy, achieving a much larger ROM than the single joints and better conditioning of the single joints over a large ROM. This ability is achieved by distributing the overall rotation of the humerus to contributions of all shoulder joints. With the exoskeleton, we wanted to support the physiological human shoulder synchronization such that patients can relearn a healthy coordination pattern (R-E). In addition, we strived to achieve similar benefits for ROM and kinematic conditioning of the robot as observed in the human shoulder (R-B). The large ROM of the humerothoracic rotation is owed to the joint contribution of the sternoclavicular and glenohumeral rotation. The primary function of the shoulder is to define the orientation of the upper arm. Hence, the upper arm orientation defined by the plane of elevation, angle of elevation, and internal/external rotation should determine the shoulder girdle angle.

The coupling of the scapula rotation on the thoracic wall as a function of the angle of elevation was the subject of many publications [53], [54] and was successfully used by Kim et al. on an exoskeleton [27]. However, the GED joint of ANYexo represents the sternoclavicular rotation and not the scapulothoracic rotation. We could not find continuous descriptions of the sternoclavicular rotation w.r.t. the humeral movement in related work. Therefore, we measured two participants' GED and AOE movements without impairment using motion capture. Onto this data, we fitted a quadratic curve to derive the nominal GED joint position for a given upper arm orientation $\theta_{\mathrm{GED,nom}}$ (parametrization in degrees). More details to the measurement and the fitting procedure can be found in our previous work [44]

$$\theta_{\mathrm{GED,nom}} = f_{\mathrm{GED}}(\theta_{\mathrm{AOE}}) = \begin{cases} -0.0053\theta_{\mathrm{AOE}}^2 - 0.0162\theta_{\mathrm{AOE}} + 20.5, & \text{if } \theta_{\mathrm{AOE}} \leq 96^\circ \\ -30.5, & \text{otherwise.} \end{cases} \tag{3}$$

The shoulder protraction/retraction is more task-dependent. Hence, an empiric method to fit a trajectory would be task-dependent. To model this behavior roughly, a linear relation of θ_{GPR} to θ_{POE} was chosen tuning the sensitivity w.r.t. θ_{POE} changes for subjective comfort of one person and kinematic conditioning. In addition a scaling with the sine of θ_{AOE} was added to avoid issues in the singularity of the CJC coordinates at $\theta_{\mathrm{AOE}} = 0^\circ$ or

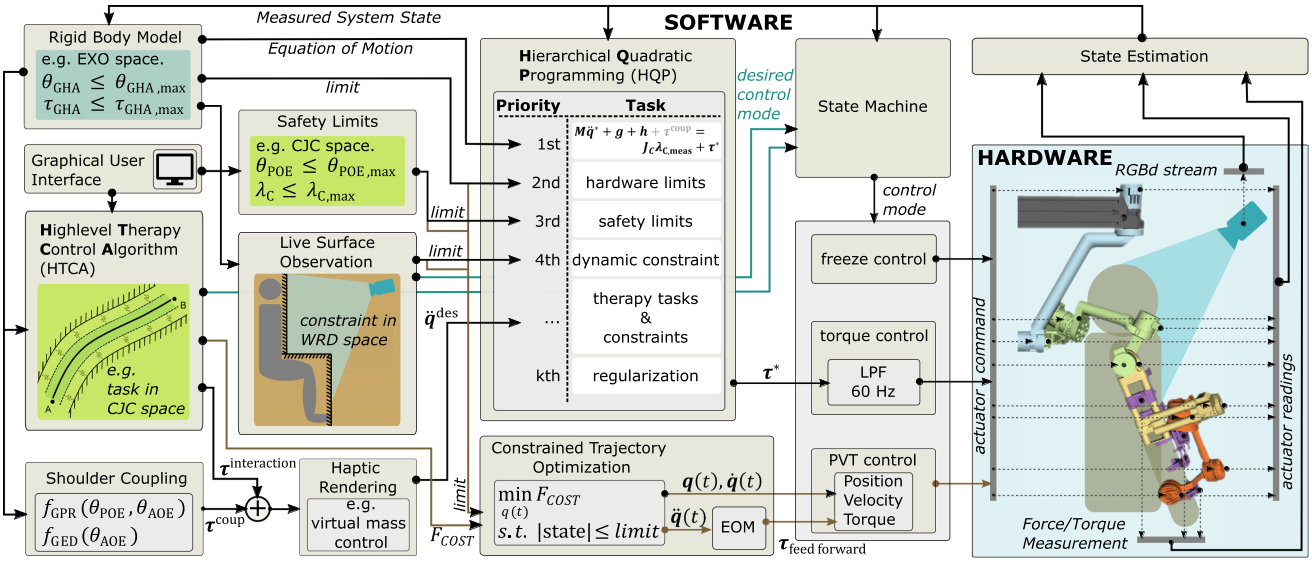

Fig. 6. Controls overview of ANYexo 2.0 with an exemplary setup of a control loop involving a Highlevel Therapy Control Algorithm (HTCA), Live surface observation [47], hierarchical quadratic programming (HQP) [42], shoulder coupling using (5) and (6), and various static limitations from robot model and safety settings. An alternative control scheme (brown arrows) could be used to control the robot's position to follow a trajectory that was optimized under constraints. HTCA or safety functions like the Live Surface Observation can request a desired control mode (blue arrows) via a state machine.

$\theta_{AOE} = 180\,°$.

$$\theta_{GPR,nom} = f_{GPR}(\theta_{POE}, \theta_{AOE}) = \begin{cases} -0.49\theta_{POE}\sin(\theta_{AOE}) + 20, & \text{if } \theta_{POE} \leq 135\,° \\ -46, & \text{otherwise.} \end{cases} \tag{4}$$

The SC joints of the robot were then controlled to follow this nominal coupled position by means of an impedance controller

$$\tau_{GPR}^{coup} = k_{GPR}(\theta_{GPR,nom} - \theta_{GPR}) - d_{GPR}\dot{\theta}_{GPR} \tag{5}$$

$$\tau_{GED}^{coup} = k_{GED}(\theta_{GED,nom} - \theta_{GED}) - d_{GED}\dot{\theta}_{GED} \tag{6}$$

where k_i and d_i are spring and damping coefficients, respectively. The stiffness and damping constants were chosen as a compromise between allowing deflections to account for individual shoulder synergy and guidance by the robot: $k_{GED} = 60\,\text{Nm/rad}$, $d_{GED} = 4\,\text{Nm/rad/s}$ and $k_{GPR} = 100\,\text{Nm/rad}$, $d_{GPR} = 10.2\,\text{Nm/rad/s}$, respectively.

B. Trajectory Generation

The conversion Jacobians were used to efficiently implement position, velocity, and acceleration constraints in CJC in optimization algorithms, e.g., for trajectory generation. Thereby, cost function elements as well as constraints could be implemented modularly in the representation space, where they were most intuitive (e.g., EXO, CJC, HND) and were merged for optimization [see Fig. 6]. Next to assuring compliance with physical boundaries and safety settings, limitations and costs can be used to, e.g., control the behavior of the system in the proximity of task space singularities.

C. Selective Compliance in Position Control

Series elastic actuators and pseudodirect drives, like those used on the ANYexo, have inherent compliance and cause low reflected inertia at the joint. Thereby, the occurring forces in case of collisions with a human are mitigated (e.g., impact or clamping). However, accurate trajectory tracking, robust to strong disturbance forces from the human arm, might be required for some therapy applications. Common solutions to achieve this performance are a high impedance for position control and integral control policies. However, as elaborated before, a low impedance during collisions might be beneficial for safety reasons. The force/torque-sensors on the ANYexo 2.0, monitoring all interaction forces between the user's arm and the robot, allowed us to distinguish between disturbances from the user's arm and external disturbances that did not act on the instrumented attachment points (e.g., therapist interactions or collisions with user's torso). The known joint torques $\tau_{\text{feed-forward}}$ to counteract the measured interaction $\mathbf{J}^\top\lambda$, Coriolis and centrifugal terms $\mathbf{h}$, and the gravity terms $\mathbf{g}$ were used as feed-forward terms for the position, velocity, and torque controller [see Fig. 6, PVT-control]. Consequently, high impedance for disturbances acting on the attachment points is achieved, while the robot reacts compliant to any other disturbance

$$\tau_{\text{command}} = \tau_{\text{feed-back}} + \tau_{\text{feed-forward}} = \tau_{\text{feed-back}} + \mathbf{J}^\top\lambda + \mathbf{h} + \mathbf{g} \tag{7}$$

where $\tau_{\text{feed-back}}$ can be any feedback policy to control position and velocity. Here, a simple PID-controller was used.

D. Hierarchical Quadratic Programming

We strove for a control framework that allows to define single methods modularly and in an intuitive as possible way. Therefore, hierarchical quadratic programming (HQP) was used

to optimize the robot behavior given various modularly defined tasks and constraints with a strictly prioritized hierarchy. For HQP, linear equality and inequality constraints for the optimization vector ξ are formulated and assigned a priority (i.e., $\mathbf{A}\xi = \mathbf{b}$ and $\mathbf{C}\xi \leq \mathbf{b}$). In our implementation, the optimization vector consisted of generalized accelerations $\ddot{\mathbf{q}}^*_{\text{EXO}}$ and torques τ^*_{EXO}. The HQP algorithm stacks all equality and inequality constraints of one priority level and computes the optimum least squares solution within the null-space of higher priority constraints. Thereby, the system controlled by the optimized torques τ^*_{EXO} will comply with the equality and inequality constraints on as many priorities as possible. We refer the interested reader to Bellicoso et al. [55] who describe the HQP in more detail for the application case on a quadruped robot.

The properties of HQP are handy to feedback linearize the physical properties of the robot, comply with safety constraints protecting the user and hardware, and execute tasks defined by high-level therapy control algorithms (HTCA) [22]. The derived Jacobians for the CJC allow the HTCA to define tasks and constraints in these coordinates that are typical for physical therapy and not specific to the robot's kinematic. This feature is particularly beneficial if the same HTCA should be transferable to different robots. In one application of the ANYexo 2.0, all haptic interactions desired by the HTCA were superposed to one desired interaction torque vector τ_{CJC} and a haptic rendering controller for tracking was used, as shown by Zimmermann et al. [42]. The output of the haptic rendering controller was then formulated as a task for the HQP [see Fig. 6].

One option to implement the shoulder coupling while using HQP was adding the coupling torques $\tau^{\text{coup}}_{\text{GPR}}$ and $\tau^{\text{coup}}_{\text{GED}}$ to the equations of motion on highest priority, see gray font in Fig. 6. This method would result in a behavior of the system similar to mechanical coupling of the shoulder, as the coupling is prioritized over any safety constraints and therapy tasks. This prioritization might be disadvantageous, as in most cases the safety constraints should be prioritized before the coupling impedance. The preferred option to implement the shoulder coupling on the ANYexo 2.0 was to superpose the coupling torques to the desired interaction torques $\tau^{\text{interaction}}$ defined by the HTCA before sending them to the haptic rendering [see Fig. 6].

To optimize energy usage and reduce noise emission, we filtered the optimized torque with a Butterworth filter with cutoff frequency at 60 Hz to comply with the torque control bandwidth of the actuators before being sent as actuator commands [see Fig. 6]. The coordination with HQP was used if some DOF were not fully controlled by the robot (i.e., partial or complete free-space rendering) and the robot was torque controlled. Else, we used a constrained optimization to compute the desired robot joint trajectory that the robot would track with joint position control [see Fig. 6].

V. Experiments

We performed a series of simulation and hardware experiments to evaluate the ANYexo 2.0 concerning the technical feature requirements presented in Section II.

TABLE II
Grid Boundaries and Resolution for ROM and Manipulability Analysis

joint	min	max	step
POE	-90	180	15
AOE	15	165	15
IER	-135	135	15
WPS	-80	80	20
WFE	-80	80	20
WUR	-30	40	5

A. Kinematic Properties

The ROM and the kinematic conditioning of the shoulder joint group (5-DOF) and the wrist joint group (3-DOF) are highly dependent on the full configuration of the respective joint group. Hence, analyzing the maximum ROM of isolated single joints is far less representative than analyzing the kinematic structure concerning the complete joint configuration. The ROM and kinematic conditioning of ANYexo 1.0 with a fixed shoulder joint was presented by Zimmermann et al. [22] using a Mollweide projection introduced by Stienen et al. [56]. For the analysis of the coupled shoulder, we used the same diagram while we developed a similarly intuitive display method for the wrist. Both visualizations allow displaying a scalar property in color on a 3-D grid of clinical joint coordinates, as seen in Fig. 7.

The data for this visualization were generated using the physics simulation of the robot. The grid positions, resulting from the parameters reported in Table II, were each set as a target position sequentially. If the point in clinical joint coordinates would lie outside of the robot's range, or the robot could not reach the target position due to any reason, the target position was omitted. For the analysis with the diagrams, any data points where all joints have less than 1° distance from the gridpoint on the diagram were considered and averaged. The kinematic conditioning of the shoulder and wrist was evaluated with the manipulability metric μ_{F}. For the shoulder, the coupled manipulability μ_{C} was reported as well. For both manipulability metrics, a value of 0 denotes a locked DOF (bad), while 1 denotes full manipulability (good) for the coupled manipulability, and values bigger than 1 mean enhanced manipulability by the coupling (better)

$$\mu_{\text{F}} = \prod_{i=1}^{3} \sigma_{\text{i}}, \qquad \mu_{\text{C}} = \prod_{i=1}^{3} \hat{\sigma}_{\text{i}} \tag{8}$$

where σ_{i} are the singular values of $\mathbf{J}^{\text{EXO}}_{\text{r,H}}$ for the shoulder and the singular values of the Jacobian $\mathbf{J}^{\text{EXO}}_{\text{r,Hand}}$ for the wrist that maps the wrist velocity in EXO space to the hand rotational velocity in WRD, i.e., $\dot{\mathbf{x}}^{\text{WRD}}_{\text{r,Hand}} = \mathbf{J}^{\text{EXO}}_{\text{r,Hand}}\dot{\tilde{\mathbf{q}}}$. For the coupled manipulability the singular values $\hat{\sigma}$ are computed from $\mathbf{J}^{\text{EXO,coup}}_{\text{r,H}}$ for the coupled shoulder. The definition and computation of the shoulder Jacobians can be found in Appendix A.

B. Available Interaction Torques

The maximum available interaction torque with the user at different shoulder poses was computed using numeric optimization. The optimization searched for the maximum and

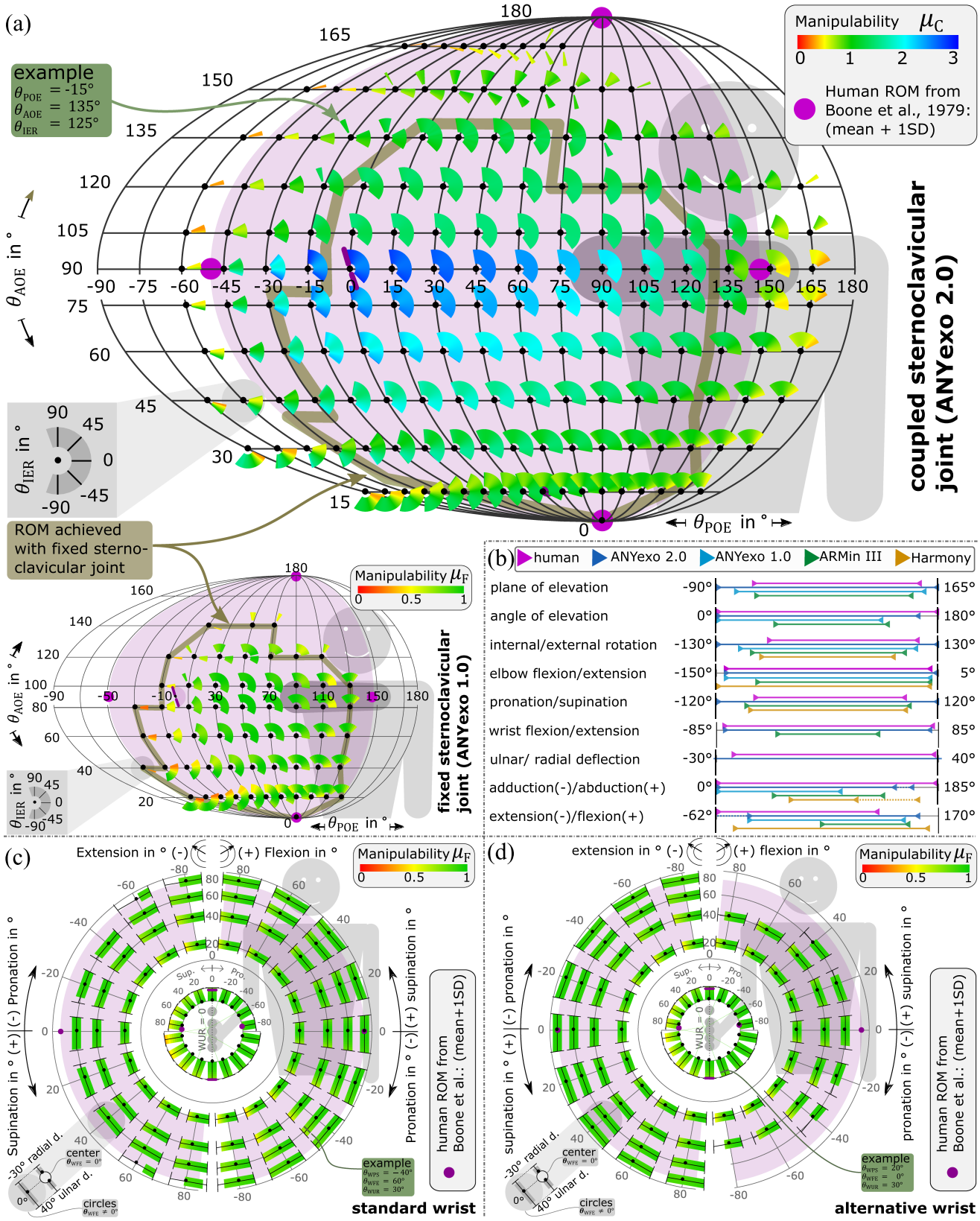

Fig. 7. Simulated kinematic properties of ANYexo 2.0. The purple color markers indicate the mean +1SD active ROM of humans without impairment according to Boone et al. [57]. The purple shades represent the extrapolated active ROM from these data points. (a) ROM and manipulability for the actively coupled shoulder in the top graph and for the fixed SC-joint (i.e., $\theta_{GPR} = \theta_{GED} = 0$) in the left lower graph. (b) Comparison of the maximum ROM in different directions by humans and exoskeletons [22], [23], [26], [57], [58]. The dotted lines in adduction/abduction and extension/flexion correspond to a less strict execution of the clinical assessment movement in the robots. (c), (d) ROM and manipulability for standard wrist and alternative wrist configuration, respectively.

minimum transmittable torque in a CJC direction while zero torque is transmitted in the other CJC directions. At the same time, the optimization considered the pose-specific gravitational load of the robot, which was recorded during the simulation experiment described in Section V-A. This isolated torque capability was reported, as this is of higher relevance for haptic rendering in training exercises than the unconditional maximum torque in any direction. An additional experiment demonstrating the capability to move a passive mass mimicking the load of a 95th percentile male arm on the shoulder joints can be found in the appended material. The wrist joints did not require a numeric analysis as the available torques were three times higher than the strength of the average human wrist and the gravity load was small at the end of the kinematic chain.

C. Activities of Daily Living

The kinematic analysis in the simulation provides a dense representation of the workspace. However, this analysis only considers the robot on its own. To analyze the ROM of the human user with the robot attached, we performed a set of 15 ADL while attached to the robot in free-space mode (e.g., transparency). In a real therapy scenario, the free-space mode would be replaced by an assistance controller (e.g., arm gravity compensation) or a trajectory controller to passively move the patients arm. However, to evaluate if the robot's kinematic structure allows us to train ADL, the free-space controller suffices for this experiment. This experiment was performed by one of the authors and main developers of ANYexo 2.0: male, with no impairments, and body height of $1.82\,\mathrm{m}$. With this choice of user, we expect the maximum performance of the robot's kinematic structure to be represented better than with a layman user. Further, ADL demonstrations with this user and an additional female user are documented by video. For the female user, the videos were recorded on the first day of using the robot.

We selected the ADL to span a ROM as diverse as possible [see Fig. 9] while involving interactions with the environment or the own body. Some of the selected ADL could be trained with real settings, e.g., wiping mouth and throuser pockets, while others would require a mock setup, e.g., perineal care and seat belt. During the ADL performance, the joint positions were recorded to extract postures of interest in postprocessing. Next to these 15 ADL, the same user performed a body washing movement, a one-sided breaststroke (i.e., swimming movement), and perineal care to demonstrate trajectories spanning a large part of the shoulder ROM.

D. Selective Compliance in Position Control

The effect of compensating the measured interaction wrench for position control as described in (7), was investigated in a trajectory tracking experiment. Therefore, a minimum jerk reference trajectory for a horizontal adduction/abduction movement from $\theta_{\mathrm{POE}} = -30^\circ$ to 130° was tracked by the robot using the controller in (7). Therefore, the other DOF were controlled to ($\theta_{\mathrm{AOE}} = 90^\circ$, $\theta_{\mathrm{IER}} = 0^\circ$, $\theta_{\mathrm{EFE}} = -45^\circ$, and all WR joints at 0°). In the first condition, the measured interaction forces are compensated $\lambda = \lambda_{\mathrm{measured}}$ (interaction aware) and in the second the measured interaction forces are not compensated $\lambda = \mathbf{0}$. During the tracking of the trajectory, a weight of $2.5\,\mathrm{kg}$ was attached to the hand attachment point suspended by a carabiner and a rope. This experiment was chosen as a demonstration of the many opportunities that the combination of precisely torque controlled joints, and interaction force measurement offer.

VI. Results

A general impression of the robot's design and performance is provided in this video https://youtu.be/pMKoDeaS37k.

A. Kinematic Properties

1) Shoulder: In comparison to the ANYexo with fixed SC-joint, the isolated θ_{POE} and θ_{AOE} ROM of the ANYexo was enhanced by about 40% and 25%, respectively, by coupling the SC-joint's movement to the humeral orientation. The θ_{IER}-ROM was increased as well by the coupling, e.g., for the fixed shoulder only 30° θ_{IER}-ROM was left at $\theta_{\mathrm{POE}} = -30^\circ$ and $\theta_{\mathrm{AOE}} = 60^\circ$ while the θ_{IER}-ROM for the coupled shoulder spanned 90° at the same configuration. Gaps in the θ_{IER}-ROM were observed at $\theta_{\mathrm{AOE}} \geq 120^\circ$. Hence, the CJC-ROM of the robot was non-convex. In general, the coupling extended the ROM in all directions on the θ_{POE}-θ_{AOE} grid, enabling the exoskeleton to reach the active ROM of 84% of the population for all directions except in positive AOE direction and negative IER direction [see Fig. 7(a), (b)]. Simultaneously the coupling maintained the manipulability of the GH-joint close to one over the majority of the θ_{POE}-θ_{AOE}-grid, resulting in an overall θ_{IER}-ROM bigger than 120°.

The GH-joint's kinematic structure was well-conditioned at the center of the robot's ROM in both the fixed and the coupled shoulder. For high AOE and low POE, we observed a girdle with decaying manipulability (i.e., $\mu \leq 0.5$) with a width of approximately 20°. This weakly conditioned girdle is only pushed outwards by the coupling while not notably gaining in width, resulting in a large well-conditioned space in the middle of the robot's ROM. While $0 \leq \mu_{\mathrm{F}} \leq 1$, $\hat{\mu}_{\mathrm{C}}$ is not bound to 1 as the rotation contribution from the SC-joint increases the clinical joint rotations per GH actuator rotation. Hence, an augmentation of the manipulability is observable in the area where the coupling is active. For $\theta_{\mathrm{AOE}} > 90^\circ$ GED did not elevate further due to the joint's end-stops. Hence, a sharp difference in manipulability occurred compared to lower AOE. Similar for $\theta_{\mathrm{POE}} > 135^\circ$, the coupling from GPR ends. A direction-specific analysis of the manipulability is in the appended material.

The available rotation velocity in all humeral rotation directions was around $6\,\mathrm{rad/s}$ where $\mu \approx 1$. This speed was around double the maximum speed the average human uses during ADL (see Table III). For areas where the coupling was active, the coupled directed manipulability (graphics in appended material) was used as a scaling factor to estimate available rotation speeds from the maximum joint speed. Values of up to $12\,\mathrm{rad/s}$ in world x-direction and up to around $9\,\mathrm{rad/s}$ for world z-direction were found.

TABLE III
MAXIMUM SPEEDS AND TORQUES. HUMAN VALUES ARE FROM ROSEN ET AL. [38] FOR THE SPEEDS, FROM HOGREL ET AL. [59] FOR THE SHOULDER TORQUE, AND FROM PLEWA ET AL. [60] FOR THE WRIST TORQUE. FOR THE SPHERICAL JOINTS THE MAXIMUM SPEEDS AND TORQUES IN ANY DIRECTION IS REPORTED TO AVOID CONVERSION BETWEEN DIFFERENT COORDINATE SYSTEMS. PEAK TORQUES ARE MARKED BOLD AND NONIMAL TORQUES ARE MARKED ITALIC. FOR HARMONY ONLY NOMINAL TORQUES WERE REPORTED IN LITERATURE [23]. ANYEXO COULD PROVIDE HIGHER NOMINAL TORQUES THAN REPORTED IF ADDITIONAL COOLING WAS USED, E.G., A FAN.

maximum ADL speed in $^\circ\,\mathrm{s}^{-1}$

	mean human	ANYexo	ARMin III [26]	Harmony [23]
GH	172	344	155	-
EB	173	688	144	-
WR	486	1719	197...1451	-

maximum isometric torque in $\mathrm{N\,m}$

	mean human	ANYexo	ARMin III [26]	Harmony [23]
GH	**53.9(m:73.5)**	**77** / *30*	**60...82** / *11...23*	*34*
EB	**55.2(m:70.9)**	**39** / *15*	**59** / *11*	*13*
WR	**8.5(m:10)**	**23** / *7*	**51** / *3...7*	*1.3*

2) Elbow: The ROM of the robot's elbow reaches from -145° to 4°, which covers the mean +1SD active ROM of humans according to Boone et al. [57].

3) Wrist: The wrist in standard configuration covered the active ROM humans without impairment (mean+1SD) according to Boone et al. [57] with two exceptions [see Fig. 7(b), (c)]. First, the extension was slightly restricted independent of the configuration of the other joints. Second, the ulnar bend was slightly restricted at strong pronation and when flexing the wrist. For the alternative wrist configuration, there was a larger gap in the ROM for high flexion particularly when combined with marked pronation or supination. In return, more extension was achievable. For both wrist configurations, the wrist's kinematic structure was mostly close to the maximum manipulability $\mu_\mathrm{F} \approx 1$ [see Fig. 7(c), (d)]. Therefore, the available wrist speed in any direction was close to 30 rad/s, which is more than three times higher than the maximum speed the average human uses during ADL, see Table III.

B. Available Interaction Torques

The shoulder of the exoskeleton needs to compensate for large torques caused by the weight of the robot arm components. These torques mainly acted in AOE direction, which was affecting the available torques in this direction [see Fig. 8]. In the majority of the ROM, transmitting interaction torques to the human in the range of the average human isometric strength should be possible, see Table III. The elbow was directly actuated with 39 Nm peak torque, the maximum gravity load from the wrist was 7 Nm. Hence, more than 32 Nm of interaction torques were available in all configurations.

C. Activities of Daily Living

The ROM of ANYexo encompassed the most critical upper-limb ADL that were extracted from Aizawa et al. [62], Magermans et al. [63], and Gates et al. [52] [see Fig. 9(a)]. Only perineal care from Aizawa et al. [62] was outside. However, perineal care could be trained with the ANYexo while the required ROM matched with the one reported by Magermans et al. [63] [see Fig. 9(a)].

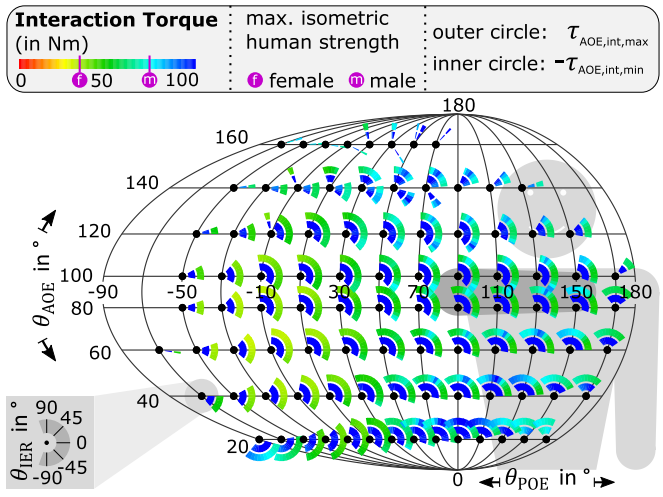

Fig. 8. Available interaction torques in AOE direction while rendering zero interaction torque in other directions. Compared to maximum isometric strength of humans with and without impairment according to Hogrel et al. [61].

All 15 chosen ADL **A** to **N** could be performed by the user. Some of them involved successful interaction with real objects and the own body [see Fig. 9(b)]. We selected some distinct joint configurations of these ADL to visualize typical postures w.r.t. the ROM of the shoulder, elbow, and wrist [see Fig. 9(c)]. Video documentation of these 15 ADL and additional ADL demonstrating interaction with objects and the own body can be found here https://youtu.be/qhs2MVgDvWc.

D. Selective Compliance in Position Control

The maximum deflection of the robot from the nominal angle of elevation (i.e., $\theta_{\mathrm{AOE}} = 0^\circ$) after attaching the disturbance weight was 11° for the controller without feedforward compensation of the interaction forces and 1° for the controller with feed-forward compensation [see Fig. 10]. Video documentation of this experiment and an experiment with static reference position tracking and dynamic disturbance is provided here https://youtu.be/63PjB3nqUEg.

VII. DISCUSSION

Devices achieving a subset of the *technical feature requirements* (see Section II) or a subset of the *Performance Goals for Clinical Adoption* (see Section I-A) were already presented in related work. However, one device that can accompany a patient from the severely affected state to full recovery for most exercise types was not available to our knowledge. ANYexo closes this gap with only minor restrictions for some exercise types.

A. Robot Structure

The ANYexo 2.0 is the first exoskeleton to implement all nine relevant DOF of the human upper limb with actuated joints that are strong enough for passive mobilization and strength training. The exoskeleton structure assures full control over the

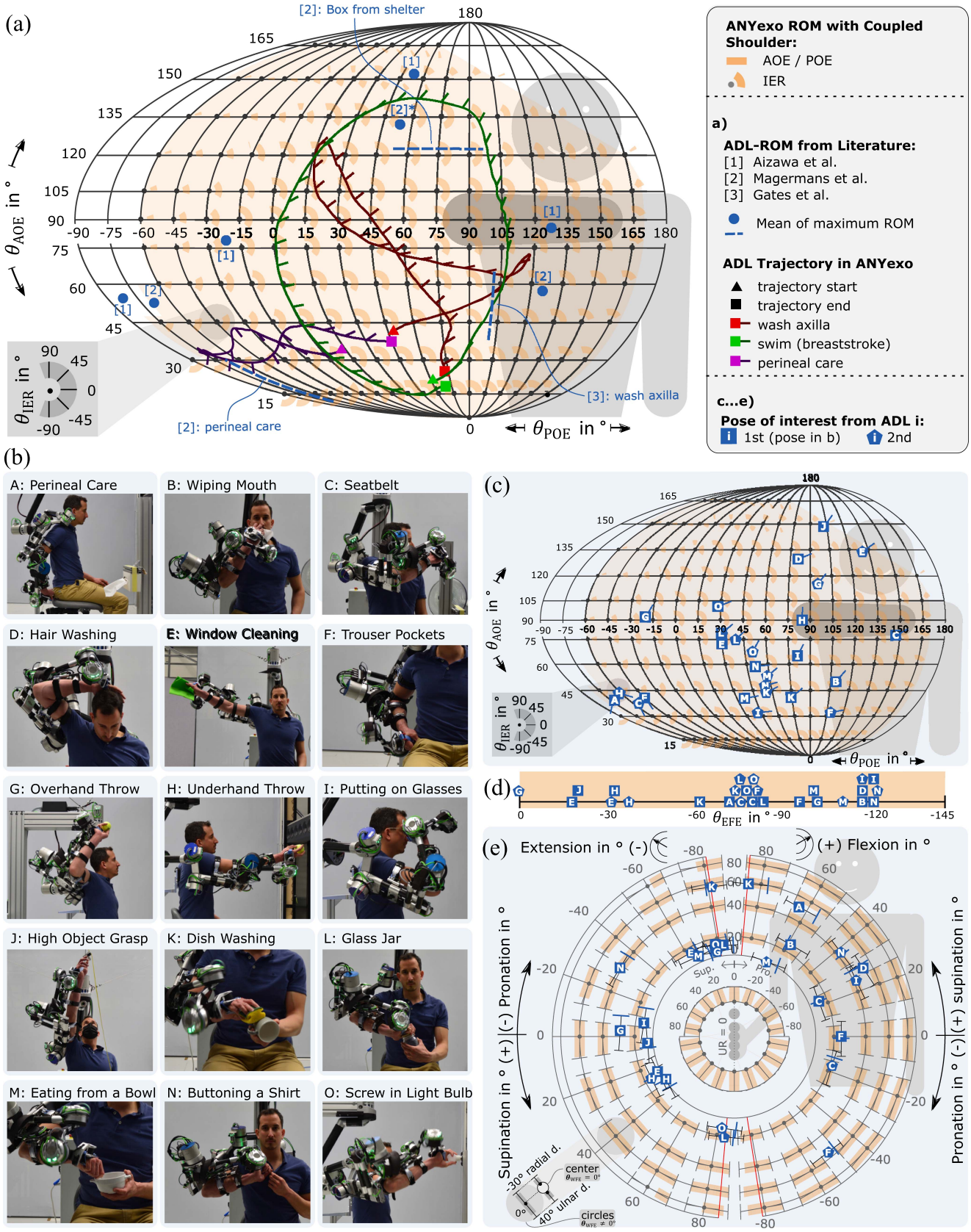

Fig. 9. Comparison of ANYexo 2.0 ROM with ADL. (a) Comparison with ADL reported by Aizawa et al. [62], Magermans et al. [63], and Gates et al. [52] as well as example trajectories for the shoulder joint. (b) Demonstration of ADL including real object interaction. The images correspond to the first pose of interest. (c)–(e) Poses of interest as snapshots from the trajectories recorded while performing the 15 ADL, see (b). The poses of interest were selected to span a large ROM in shoulder (c), elbow (d), and wrist (e).

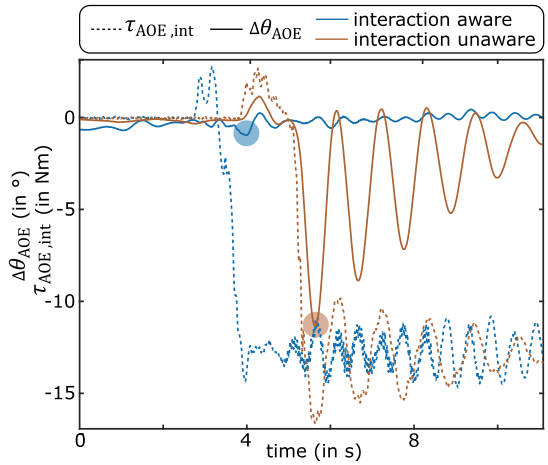

Fig. 10. Comparison of the performance of a position tracking controller with or without compensation of the measured interaction forces when mounting a 2.5 kg disturbance weight, swinging on a rope, to the hand attachment point during trajectory tracking. $\tau_{AOE,int}$ is the reflected measured interaction torque in AOE-direction.

redundancy of the human arm during activity-oriented training and allows defining the configuration of all joints for joint-oriented training. Thus, the ANYexo can correct for undesired compensation movements to train physiologic synergies and distributes the interaction load over multiple limb segments.

Many of the 15 demonstrated ADL resulted in a remarkable movement in ulnar and radial deviation (e.g., G, I, O, L, M, and K) and wrist flexion/extension (e.g., N, K, A, D, and F), which indicates the relevance of these DOF for ADL which are often neglected in exoskeletons (e.g., [23], [26]).

B. Range of Motion

The ANYexo 2.0 with the coupled sternoclavicular joints could achieve almost the full, conservatively extrapolated, active ROM of humans without impairment that was derived from the mean +1SD independent joint ROM reported by Boone et al. [57]. In contrast, with fixed sternoclavicular joints a much smaller ROM could be covered [see Fig. 7(a)]. The ANYexo 2.0 reached or exceeded all of these individual active ROM at some configurations of the arm, except for angles of elevation (AOE) higher than $165°$. Further, the active ROM in isolated directions could be reached at the reported clinical assessment arm position, except for internal shoulder rotations (IER) lower than $-45°$, and wrist extension (WFE) lower than $-60°$. However, the maximum wrist extension angles of the human active ROM can be reached with the alternative configuration of the wrist [see Fig. 7(e)]. Further, internal shoulder rotations exceeding $-90°$ can be trained in many poses of the shoulder other than the typical clinical ROM assessment pose. Thus, the device's ROM allowed joint-oriented training with mildly affected patients even close to the border of the active ROM of humans without impairment.

Thereby, the robot's ROM allowed training of most ADL of the upper limb, which are typical for occupational therapy (e.g., task-oriented movements). The demonstration of 15 ADL, including interaction with the own body and real objects, proved that the required ROM could be reached and traveled through a user while being attached to the robot [see Fig. 9]. Thus, the parts of the conservatively extrapolated human active ROM that could not be reached with the exoskeleton, did not affect the ability to perform ADL. This finding indicates that most other users could execute this set of ADL with the robot, as long as the robot is adaptable to their size. Further, the experiment demonstrates that the kinematic structure and link design avoid collisions with the human body in the ROM required for various ADL. However, for significantly smaller users, the ROM might be smaller as all robot components are closer to each other and closer to the user's torso. For the performed ADL, we could observe a tendency of more external rotation with increasing θ_{POE} and θ_{AOE}, which coincides with the findings of Georgarakis et al. [20]. This characteristic shoulder synergy is supported by the kinematic properties of ANYexo 2.0 that shift the θ_{IER}-ROM toward external rotation for high θ_{POE} and θ_{AOE}. All DOF of the wrist were used during the execution of the 15 ADL indicating the relevance of a 3-DOF wrist.

The ROM required for essential ADL like perineal care (A), fastening a seat belt (C), reaching into the trouser pockets (F), and reaching a high cupboard (J) was enabled by coupling the humeral orientation of the robot with the shoulder girdle movement inspired by the coupling of the human shoulder [see Fig. 7(b) and Fig. 9]. Thus, leveraging the shoulder coupling improved the applicability of ANYexo.

The restriction to angles of elevation lower than $165°$ and the bounded internal/external rotation at some poses of the arm clearly restricts the ROM of users without impairment. However, these restrictions might not be relevant for task-oriented therapy, as many ADL could be performed without these regions of the active ROM. A more extensive set of ADL would have to be tested to identify if the remaining restrictions in the ROM are relevant for task-oriented therapy.

The design of the attachment points and the placement of the actuators and links enabled a body-proximal ROM of the robot that allows starting the training for severely affected patients in their typical active ROM.

The ANYexo 2.0 reached or exceeded the ROM of ARMin III...V [see Fig. 7(b)]. It is difficult to compare the ANYexo's ROM to other exoskeletons in related work as mostly only extremal positions have been reported quantitatively and not the ROM in all configurations. However, the ANYexo 2.0 and the Harmony were close to covering the human shoulder's extremal points of the active ROM. The ANYexo 2.0 excelled in internal/external shoulder rotation and adduction, while Harmony reached higher angles of elevation. Both devices showed a restricted abduction when external rotation was not allowed. However, the ANYexo could abduct $32°$ more in this case.

C. Training Interaction With Real Environment

The body-proximal ROM and the open hand design allowed ADL with body interaction, e.g., wiping mouth (B), washing hair (D), putting on glasses (I), and buttoning a shirt (N). These intimate ADL are essential to relearn for patients to regain

autonomy in daily life. Other ADL could be demonstrate that involved direct interaction with real objects, e.g., opening a glass jar (L) or donning a seat belt (C). ADL training with real objects and real interaction with the ANYexo might facilitate the transfer of the learned skills in therapy to living at home. This transfer has been suggested to contribute substantially to the retention of training effects after the therapy ended [9].

The *ADL* experiment were performed by one of the main developers with experience in interacting with the robot. It is unclear, if other users could perform the same ADL and if they would use the same ROM. However, the female participant shown in the videos could familiarize with the robot in a short time. She demonstrated successful performance in multiple ADL as documented by video (see video ROM and video ADL[1]). Thus, lets assume that layman would be able to perform the set of 15 selected ADL. However, a larger study involving a representative participant cohort without experience would be required to confirm. Further, the robot was used in transparent mode, while in a typical therapy setting, guidance, assistance, or resistance would be provided by the robot.

D. Speed and Strength in High-Quality Haptic-Rendering

The extracted poses of the 15 ADL, which were chosen in extreme ROM positions, as well as the three, reported ADL-trajectories, are not located in the areas with low manipulability [see Figs. 7(a) and 9]. Thus, the kinematic structure offers high and almost isometric controllability for free-motion rendering (i.e., haptic transparency) and freedom of movement during ADL.

Training ADL at full speed is a core requirement. However, barely enabling the robot to move at this speed led to a feeling of speed restriction in users of our previous prototype ARMin III [26]. This observation can be explained by the actuation margin the robot needs to render free-space or the desire of users to move faster than the average human would during ADL, e.g., to train reactions. With the controlled coupling of the shoulder, speeds higher than twice the speed required for ADL [38] were supported by ANYexo 2.0. Hence, the achievable maximum speed is around twice as high than for comparable devices, e.g., ARMin III [26], ArmeoPower (Hocoma AG, Switzerland), and Harmony [23] (estimated from video), see Table III. Further, the free-motion rendering on ANYexo is quite independent of the speed [42] while others found a linear relationship of the resistance to speed [23]. Thus, this capability should allow training ADL with low resistance at the speed of humans without impairment, as indicated by Zimmermann et al. [42] and the ADL experiments in this work. The powerful series-elastic and quasi-direct actuated joints provide robust and accurate joint torque control. The consequent instrumentation of all human–robot contact points and full controllability of the robot's dynamics enabled closed-loop control of interaction forces with accurate feedback linearization. Thereby, even parts of the robot's inertia can be compensated in free-space (transparency) rendering [42].

[1][Online]. Available: https://youtu.be/pMKoDeaS37k at 195 s and 291 s, respectively

Even though the supported velocity of the robot is far below the capability that humans show in sports [39], [40], [64], training above the regular velocities in ADL will lower the feeling of being restricted by the robot. Thereby, moderately and mildly affected patients might regain sufficient speed for fast reactions (e.g., catching a falling object).

Unlike conventional therapy appliances or passive devices like the ArmeoSpring (Hocoma, Switzerland), the exoskeleton allows to adapt the resistance or assistance without the therapist's actions and can correct (guide) the movement execution. The strength of the device should suffice to mobilize 95th-percentile male arms in the full ROM. Further, maximum isometric torque training of the shoulder and wrist would be possible for most users in various arm postures, except for pressing in the direction of negative angle of elevation. The nominal power of the drives was 240 W for each shoulder and elbow actuator and 200 W for each wrist actuator. Thus, demanding endurance strength training could be performed with ANYexo, given that the average overall power an adult male can produce while rowing is 195 W [65]. For extensive strength training, the drives would require additional heat sinks (e.g., fans). To mobilize a passive 95th-percentile male arm over a longer time duration and to increase the interaction force capacity in angle of elevation, a passive spring system should be added to the GED joint to compensate a part of the gravity load.

E. Human–Robot Attachment

The human–robot attachment concept involving self-adapting attachment mechanisms for different arm diameters (patent pending EP21205583.4) was designed slim enough to prevent collisions with the body of the user during activities involving body-proximal movements.

The coupled shoulder increased the ROM [see Fig. 7(a)] and comfort [23] compared to the fixed robot shoulder for users that coordinate their shoulder sufficiently themselves. However, the scapulohumeral rhythm is often attenuated for patients with impaired muscular activity in the shoulder. Hence, the coupled shoulder of ANYexo 2.0 would impose the scapulohumeral rhythm over the attachment point at the upper arm without any support of the shoulder complex between the GH and scapulothoracic joint. The scapula orthosis presented by Georgarakis et al. [43], [44] could be combined with ANYexo 2.0 to offer additional support for the scapula by stabilizing toward the thoracic wall and supporting the medial rotation of the scapula during arm elevations.

F. Intuitive, Modular and Save Implementation of Control

We proposed hierarchical quadratic programming to merge tasks and constraints in a generalized fashion while allowing formulation in the application-specific coordinate representations [22]. The presented formulation of Jacobians for the CJC enabled using hierarchical quadratic programming for typical physical therapy tasks and constraints (e.g., passive ROM defined in CJC). Further, these Jacobians can be used to describe constraints and cost in CJC for constraint trajectory optimization. This modular combination of tasks and constraints defined

in the different representation spaces EXO (i.e., robot joint limits), HND (i.e., occupational therapy task), and CJC (i.e., physical therapy task and passive ROM) allows versatile recombination of these modules by the high-level therapy control algorithm. This modularity will streamline algorithm development for individualized therapy exercises. Through introduction of methods for these modules and evaluation of their performance was/will be subject to other publications. The contribution of this article is the proposed software structure and the key methods to break down the complexity of the controller implementation for this 9-DOF robot with skewed actuation axes into single modules that can be developed more intuitively and allow recombination.

Using Jacobians to map velocities and torques between joint space and task space is common in robotics. However, the derivation of a Jacobian for the mapping between a serial robot joint space and the proposed clinical joint space containing parallel components (or shoulder coupling terms) was so far not presented to the knowledge of the authors. This mapping allows converting controller outputs defined in this standardized clinical joint space to any generalized coordinates of a serial kinematic robot, which facilitates the transfer of control methods between devices.

Body-proximal ADL can be trained with ANYexo 2.0. Thereby, undesired collisions of the robot with the head and torso of the user must be avoided. Sommerhalder et al. [47] demonstrated the use of depth sensors (IntelRealsense) for visual observation of the user's body surface and corresponding constraint definition for haptic rendering on ANYexo. Thereby, Sommerhalder et al. have demonstrated a method for online adaptive and cost-efficient collision avoidance. A proof of concept for this collision avoidance combined with body-proximal therapy exercises should be investigated in future work.

The experiment has shown that the compliance of a position controller can be more than ten times higher for unmeasured external disturbances (e.g., therapist or the user's body) than for disturbances measured by the instrumented attachment points (e.g., user's arm). Hence, the patient's arm can be guided with sufficient accuracy, even in the presence of disturbances by the arm. At the same time, the robot behaves compliant regarding any collisions with other parts than the attachment points. This selective compliance contributes to the safe operation of the robot in the proximity of the user's body. This performance is owed to the combination of precise joint torque control and interaction force measurement.

G. Performance Goals for Clinical Adoption

The ANYexo 2.0 hardware is capable to provide assessments and exercises for joint-oriented training of ROM, strength, and dynamic joint coordination for severely affected to fully recovered patients. Only minor restrictions of active ROM and maximum strength for mildly affected patients remained. Most conventional therapy methods, end-effector-based robots, and low-dimensional exoskeletons do not allow controlling the entire posture of the arm while ANYexo 2.0 covers all relevant DOF of the human arm. The ROM and speed of ANYexo 2.0 allows us to train various upper-limb ADL including real object interactions even at higher pace than typical. In contrast, other state of the art upper limb exoskeletons (e.g., ARMin III [26] and Harmony [23]) cannot provide the speed, manipulability, and/or back driveability to perform ADL at typical pace without significant restriction by the robot. The ANYexo 2.0 allows particularly for body-proximal movements to train activities with body interaction and accomodate for the typically body-proximal active ROM of severely affected patients.

VIII. Conclusion

The rehabilitation exoskeleton ANYexo 2.0 presented in this work unifies sufficient ROM, strength, speed, and haptic-rendering accuracy to provide meaningful occupational (activity-oriented) and physical (joint-oriented) therapy exercises for severely affected patients to people without impairment. This versatility, combined with the full control over all nine relevant DOF of the human upper limb, promises to achieve applicability of the device for a broad variety of therapy provided in clinics (e.g., neurological, orthopedical, and sports injury patients).

The broad applicability of this robotic system might improve the deployment and acceptance of rehabilitation robots in clinics, as therapists and patients would need to familiarize themselves only with a few devices for upper limb training. Further, therapists could delegate more of their repetitive work to robotic devices. Thereby, therapists could leverage the benefits of robot-assisted therapy, such as quantitative analysis and high amount of repetitions. These benefits might help redeem the high cost of acquisition and therapist training related to such devices. It is up to future work to determine, if devices with full control over a limb, devices acting on a single joint, or combinations are overall more effective in the clinical application.

However, to apply this robotic system for therapy, a suitable high-level therapy control algorithm and extended safety measures are required, which were not subject of this publication. Further, in the authors opinion, therapists will keep an essential role in robot-assisted therapy, despite the evolving abilities of robotic hardware and software. Many tasks in therapy can hardly be automated, ranging from interpersonal communication to physical interactions, e.g., palpation, and particularly including strategic analysis and planning of the therapy.

The precise haptic rendering and the kinematic structure optimized for manipulation make the device eligible for augmented reality haptic feedback for telemanipulation (e.g., construction or surgery) and haptic interaction with virtual environments (e.g., entertainment industry).

Appendix
Coordinate Conversions

1) Position Conversion: The three CJC angles θ_{POE}, θ_{AOE}, and θ_{IER} describe the humeral orientation w.r.t. the torso by sequential rotations along the x-axis and z-axis of the coordinate system attached to the humerus frame H [see Fig. 11]. For our application, we assume the torso at fixed pose w.r.t. the world frame. Hence, all orientations are defined w.r.t the world frame W instead of the torso frame

$$\mathbf{R}_{\mathrm{W,H}}^{\mathrm{CJC}}(\theta_{\mathrm{POE}}, \theta_{\mathrm{AOE}}, \theta_{\mathrm{IER}})$$

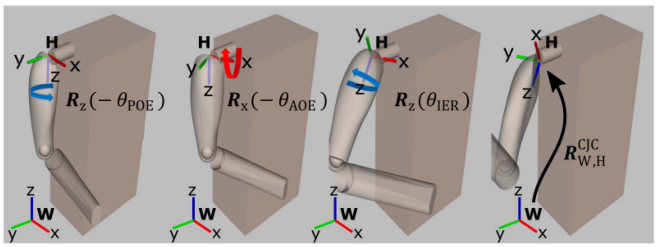

Fig. 11. Left to right: Undeflected orientation of the humerus frame (H) to rotated with $\mathbf{R}^{\text{CJC}}_{\text{W,H}}$ w.r.t the world frame (W).

$$= \mathbf{R}_x(\pi)\mathbf{R}_z(-\theta_{\text{POE}})\mathbf{R}_x(-\theta_{\text{AOE}})\mathbf{R}_z(\theta_{\text{IER}}). \tag{9}$$

The orientation of H can as well be described by using sequential EXO coordinates

$$\mathbf{R}^{\text{EXO}}_{\text{W,H}}(\theta_{\text{GPR}}, \theta_{\text{GED}}, \theta_{\text{GHA}}, \theta_{\text{GHB}}, \theta_{\text{GHC}}) = \mathbf{R}_{\text{SC}}(\theta_{\text{GPR}}, \theta_{\text{GED}})\mathbf{R}_{\text{GH}}(\theta_{\text{GHA}}, \theta_{\text{GHB}}, \theta_{\text{GHC}})\mathbf{R}_{\text{c}} \tag{10}$$

where $\mathbf{R}_{\text{SC}}$ and $\mathbf{R}_{\text{GH}}$ are the rotation contribution from the SC joints and GH joints, respectively, and $\mathbf{R}_{\text{c}}$ is a constant rotation specific for the kinematic structure of the robot. The conversion functions are found by solving

$$\mathbf{R}^{\text{CJC}}_{\text{W,H}} \overset{!}{=} \mathbf{R}^{\text{EXO}}_{\text{W,H}} \tag{11}$$

$$\theta_{\text{AOE}} = \arccos\left(-\mathbf{R}^{\text{EXO}}_{\text{W,H}}(3,3)\right) \tag{12}$$

$$\theta_{\text{POE}} = \text{arctan2}\left(\mathbf{R}^{\text{EXO}}_{\text{W,H}}(1,3), -\mathbf{R}^{\text{EXO}}_{\text{W,H}}(2,3)\right) \tag{13}$$

$$\theta_{\text{IER}} = \text{arctan2}\left(\mathbf{R}^{\text{EXO}}_{\text{W,H}}(3,1), \mathbf{R}^{\text{EXO}}_{\text{W,H}}(3,2)\right) \tag{14}$$

for $\theta_{\text{AOE}} \in (0, \pi)$, where (*j*,*i*) is the matrix component in the *j*th row and *i*th column. The conversion from CJC coordinates to the EXO coordinates is dependent on the kinematic of the robot. For ANYexo, the rotations of the orthogonal GH joints are extracted by solving

$$\mathbf{R}_{\text{GH}} \overset{!}{=} \hat{\mathbf{R}}_{\text{GH}} = \mathbf{R}^{\top}_{\text{SC}}\mathbf{R}^{\text{CJC}}_{\text{W,H}}\mathbf{R}^{\top}_{\text{c}} \tag{15}$$

$$\theta_{\text{GHB}} = \arcsin(-\hat{\mathbf{R}}_{\text{GH}}(3,3)) \tag{16}$$

$$\theta_{\text{GHA}} = \text{arctan2}(-\hat{\mathbf{R}}_{\text{GH}}(1,3), \hat{\mathbf{R}}_{\text{GH}}(2,3)) \tag{17}$$

$$\theta_{\text{GHC}} = \text{arctan2}(-\hat{\mathbf{R}}_{\text{GH}}(3,2), \hat{\mathbf{R}}_{\text{GH}}(3,1)) \tag{18}$$

for $\theta_{\text{GHB}} \in (-\pi, \pi)$. The same principle can be applied for wrist DOF conversion as WR is described by serial joints with intersecting axis for EXO and CJC coordinates.

2) Velocity Conversion: To convert efficiently between CJC and EXO velocity, we search for J_{CE} with

$$\dot{\mathbf{q}}^{(9\times1)}_{\text{CJC}} = \begin{bmatrix} \dot{\tilde{\mathbf{q}}}^{(5\times1)}_{\text{CJC}} \\ \dot{\theta}_{\text{EFE}} \\ \dot{\bar{\mathbf{q}}}^{(3\times1)}_{\text{CJC}} \end{bmatrix} = \mathbf{J}^{(9\times9)}_{\text{CE}}\dot{\mathbf{q}}^{(9\times1)}_{\text{EXO}} = \begin{bmatrix} \tilde{\mathbf{J}}^{(5\times5)}_{\text{CE}} & 0 & \mathbf{0}^{(5\times3)} \\ \mathbf{0}^{(1\times5)} & 1 & \mathbf{0}^{(1\times3)} \\ \mathbf{0}^{(3\times5)} & 0 & \bar{\mathbf{J}}^{(3\times3)}_{\text{CE}} \end{bmatrix} \begin{bmatrix} \dot{\tilde{\mathbf{q}}}^{(5\times1)}_{\text{EXO}} \\ \dot{\theta}_{\text{EFE}} \\ \dot{\bar{\mathbf{q}}}^{(3\times1)}_{\text{EXO}} \end{bmatrix}. \tag{19}$$

The derivation of $\bar{\mathbf{J}}_{\text{CE}}$ is straightforward as EFE is a unit mapping and WR is a simple spherical joint with serial DOF. For the shoulder conversion Jacobian $\tilde{\mathbf{J}}_{\text{CE}}$, the twist of the H-frame in world coordinates $\dot{\mathbf{x}}_{\text{H,WRD}}$ can be described with both joint coordinate systems using standard robotics methods to formulate the Jacobians

$$\dot{\mathbf{x}}^{WRD}_{\text{H}} = \mathbf{J}^{\text{EXO}}_{\text{H}}\dot{\mathbf{q}}_{\text{EXO}} = \mathbf{J}^{\text{CJC}}_{\text{H}}\dot{\mathbf{q}}_{\text{CJC}} \tag{20}$$

where

$$\mathbf{J}^{\text{CJC}}_{\text{H}} = \begin{bmatrix} \mathbf{J}^{\text{CJC}}_{\text{r,H}} \\ \mathbf{J}^{\text{CJC}}_{\text{p,H}} \end{bmatrix}, \qquad \mathbf{J}^{\text{EXO}}_{\text{H}} = \begin{bmatrix} \mathbf{J}^{\text{EXO}}_{\text{r,H}} \\ \mathbf{J}^{\text{EXO}}_{\text{p,H}} \end{bmatrix} \tag{21}$$

$$\mathbf{J}^{\text{CJC}}_{\text{p,H}} = \begin{bmatrix} \mathbf{A}^{(3\times2)} & \mathbf{0}^{(3\times3)} \end{bmatrix} = \quad \mathbf{J}^{\text{EXO}}_{\text{p,H}} \tag{22}$$

$$\mathbf{J}^{\text{CJC}}_{\text{r,H}} = \begin{bmatrix} \mathbf{0}^{(3\times2)} & \mathbf{C}^{(3\times3)} \end{bmatrix}, \qquad \mathbf{J}^{\text{EXO}}_{\text{r,H}} = \begin{bmatrix} \mathbf{B}^{(3\times5)} \end{bmatrix} \tag{23}$$

where $\mathbf{J}_{\text{p}}$ and $\mathbf{J}_{\text{r}}$ are position and rotation Jacobians, respectively. Using (20), the conversion Jacobian $\tilde{\mathbf{J}}_{\text{CE}}$ results in

$$\tilde{\mathbf{J}}_{\text{CE}} = \mathbf{J}^{\text{CJC}+}_{\text{H}}\mathbf{J}^{\text{EXO}}_{\text{H}} = \begin{bmatrix} (\mathbf{A}^{+}\mathbf{A})^{(2\times2)} & \mathbf{0}^{(2\times3)} \\ (\mathbf{C}^{+}\mathbf{B})^{(3\times5)} & \end{bmatrix} \tag{24}$$

$$= \begin{bmatrix} \mathbb{I}^{(2\times2)} & \mathbf{0}^{(2\times3)} \\ (\mathbf{C}^{+}\mathbf{B})^{(3\times5)} & \end{bmatrix} \tag{25}$$

where $(+)$ denotes the Moore–Penrose pseudoinverse. It can be shown that the pseudoinverse is valid for the allowed joint range $\theta_{\text{AOE}} \in (0, \pi)$ and $\theta_{\text{GHB}} \in (-\pi, \pi)$ and further

$$\tilde{\mathbf{J}}^{-1}_{\text{CE}} = \mathbf{J}^{\text{EXO}+}_{\text{H}}\mathbf{J}^{\text{CJC}}_{\text{H}}. \tag{26}$$

3) Acceleration Conversion: To convert accelerations, the derivative of the conversion Jacobian $\dot{\mathbf{J}}_{\text{CE}}$ is required, which can be computed based on the derivatives of the task space Jacobians. Hence, $\dot{\mathbf{J}}_{\text{CE}}$ consists of components that can be computed with standard robotic libraries

$$\ddot{\tilde{\mathbf{q}}}_{\text{CJC}} = \tilde{\mathbf{J}}_{\text{CE}}\ddot{\tilde{\mathbf{q}}} + \dot{\tilde{\mathbf{J}}}_{\text{CE}}\dot{\tilde{\mathbf{q}}} \tag{27}$$

$$\dot{\tilde{\mathbf{J}}}_{\text{CE}} = \mathbf{J}^{\text{CJC}+}_{\text{r,H}}\left(\dot{\mathbf{J}}^{\text{EXO}}_{\text{r,H}} - \dot{\mathbf{J}}^{\text{CJC}}_{\text{r,H}}\tilde{\mathbf{J}}_{\text{CE}}\right) \tag{28}$$

$$\dot{\tilde{\mathbf{J}}}^{-1}_{\text{CE}} = \tilde{\mathbf{J}}^{-1}_{\text{CE}}\dot{\tilde{\mathbf{J}}}_{\text{CE}}\tilde{\mathbf{J}}^{-1}_{\text{CE}}. \tag{29}$$

4) Jacobian for Coupled Shoulder: If the SC joints are coupled to the humeral rotation (see Section IV-A), the independent DOF reduce from five to three. Hence, the coupled shoulder movement in CJC can be described by $\tilde{\mathbf{J}}^{\text{coup}}_{\text{CE}}$ and the movement of the GH joints of EXO. This coupled movement description will be needed to describe the coupled manipulability of the shoulder for analysis of the kinematic properties

$$\tilde{\mathbf{J}}_{\text{CE}} = \begin{bmatrix} \mathbb{I}^{(2\times2)} & \mathbf{0}^{(2\times3)} \\ (\mathbf{C}^{+}\mathbf{B})^{(3\times5)} & \end{bmatrix} = \begin{bmatrix} \mathbb{I}^{(2\times2)} & \mathbf{0}^{(2\times3)} \\ \mathbf{D}^{(3\times2)} & \mathbf{E}^{(3\times3)} \end{bmatrix} \tag{30}$$

$$\tilde{\mathbf{J}}^{\text{coup}}_{\text{CE}} = \begin{bmatrix} \mathbf{\Lambda}\mathbf{E} \\ \mathbf{D}\mathbf{\Lambda}\mathbf{E} + \mathbf{E} \end{bmatrix} \tag{31}$$

$$\mathbf{\Lambda} = \begin{bmatrix} \frac{\partial f_{\text{GPR}}}{\partial \theta_{\text{POE}}} & \frac{\partial f_{\text{GPR}}}{\partial \theta_{\text{AOE}}} & 0 \\ \frac{\partial f_{\text{GED}}}{\partial \theta_{\text{POE}}} & \frac{\partial f_{\text{GED}}}{\partial \theta_{\text{AOE}}} & 0 \end{bmatrix} \tag{32}$$

where $\mathbf{\Lambda}$ contains the partial derivatives of the coupling functions (3) and (4). The rotation of the humerus $\dot{\mathbf{x}}_{\mathrm{r,H}}^{\mathrm{WRD}}$ with coupled shoulder is then described by

$$\dot{\mathbf{x}}_{\mathrm{r,H}}^{\mathrm{WRD}} = \mathbf{J}_{\mathrm{r,H}}^{\mathrm{EXO,coup}} \dot{\mathbf{q}}_{\mathrm{GH}}, \text{ where } \dot{\mathbf{q}}_{\mathrm{GH}} = \begin{bmatrix} \dot{\theta}_{\mathrm{GHA}} \\ \dot{\theta}_{\mathrm{GHB}} \\ \dot{\theta}_{\mathrm{GHC}} \end{bmatrix} \tag{33}$$

$$\mathbf{J}_{\mathrm{r,H}}^{\mathrm{EXO,coup}} = \mathbf{J}_{\mathrm{r,H}}^{\mathrm{CJC}} \tilde{\mathbf{J}}_{\mathrm{CE}}^{\mathrm{coup}} \tag{34}$$

where the contribution of the coupled SC joints to the velocity is incorporated by the added coupling terms in (31).

5) Torque Conversion: When applying the derived conversion Jacobian $\mathbf{J}_{\mathrm{CE}}$ to convert torques using (35), we observe that $\tau_{\mathrm{GPR}}^{\mathrm{EXO}} \neq \tau_{\mathrm{GPR}}^{\mathrm{CJC}}$ and $\tau_{\mathrm{GPR}}^{\mathrm{EXO}} \neq \tau_{\mathrm{GPR}}^{\mathrm{CJC}}$, which was to be expected due to the parallel structure of the CJC shoulder coordinates. To give an intuition: the SC-torques in EXO representation act on the SC joint and support the GH joint, the SC-torques in CJC representation are only acting on the SC joint

$$\tau^{\mathrm{EXO}} = \mathbf{J}_{\mathrm{CE}}^{\top} \tau^{\mathrm{CJC}}. \tag{35}$$

ACKNOWLEDGMENT

The authors would like to thank Robin Stähli, Patrick Bruni, Blaise Etter, Adrian Esser, Leonardo Simovic, and Florian Teuscher for their valuable contribution during their master theses. Further, they would like to thank Jaeyong Song, David Müller, Patrick Huwiler, Patrick Bösch, Giorgio Valsecchi, Konrad Meyer, Dhionis Sako, Anna-Maria Georgarakis, Farbod Farshidian, Burak Cizmeci, Michael Herold-Nadig, Marco Bader, Roland Stärk, Stefan Schneller, and Natalie Willi for their essential support of the project.

REFERENCES

[1] M. P. Lindsay et al., "World stroke organization (WSO): Global stroke fact sheet 2019," vol. 14, no. 8, pp. 806–817, 2019.

[2] V. L. Feigin et al., "Global, regional, and national burden of neurological disorders, 1990–2016: A systematic analysis for the global burden of disease study 2016," *Lancet Neurol.*, vol. 18, no. 5, pp. 459–480, 2019.

[3] S. A. Combs, S. P. Kelly, R. Barton, M. Ivaska, and K. Nowak, "Effects of an intensive, task-specific rehabilitation program for individuals with chronic stroke: A case series," *Disabil. Rehabil.*, vol. 32, no. 8, pp. 669–678, Jan. 2010.

[4] M. Rijntjes, K. Haevernick, A. Barzel, H. van den Bussche, G. Ketels, and C. Weiller, "Repeat therapy for chronic motor stroke: A pilot study for feasibility and efficacy," *Neurorehabil Neural Repair*, vol. 23, no. 3, pp. 275–280, 2009.

[5] K. Wing, J. V. Lynskey, and P. R. Bosch, "Whole-body intensive rehabilitation is feasible and effective in chronic stroke survivors: A. retrospective data analysis," *Topics Stroke Rehabil.*, vol. 15, no. 3, pp. 247–255, 2008.

[6] G. Kwakkel, B. J. Kollen, J. V. Van der Grond, and A. J. H. Prevo, "Probability of regaining dexterity in the flaccid upper limb: Impact of severity of paresis and time since onset in acute stroke," *Stroke*, vol. 34, no. 9, pp. 2181–2186, 2003.

[7] L. H. Thomas et al., "Repetitive task training for improving functional ability after stroke: A major update of a cochrane review," *Stroke*, vol. 48, no. 4, pp. e102–e103, 2017.

[8] J. Bo Nielsen, M. Willerslev-Olsen, L. Christiansen, J. Lundbye-Jensen, and J. Lorentzen, "Science-based neurorehabilitation: Recommendations for neurorehabilitation from basic science," *J. Motor Behav.*, vol. 47, no. 1, pp. 7–17, 2015.

[9] V. Klamroth-Marganska et al., "Three-dimensional, task-specific robot therapy of the arm after stroke: A multicentre, parallel-group randomised trial," *Lancet Neurol.*, vol. 13, no. 2, pp. 159–166, 2014.

[10] M. Ferreira et al., "Effectiveness of robot therapy on body function and structure in people with limited upper limb function: A systematic review and meta-analysis," *PLoS One*, vol. 13, no. 7, 2018, Art. no. e0200330.

[11] K. S. G. Chua and C. W. K. Kuah, "Innovating with rehabilitation technology in the real world: Promises, potentials, and perspectives," *Amer. J. Phys. Med. Rehabil.*, vol. 96, no. 10 Suppl 1, 2017, Art. no. S150.

[12] G. Turchetti, N. Vitiello, S. Romiti, E. Geisler, and S. Micera, "Why effectiveness of robot-mediated neurorehabilitation does not necessarily influence its adoption," *IEEE Rev. Biomed. Eng.*, vol. 7, pp. 143–153, 2014.

[13] C. Celian et al., "A day in the life: A qualitative study of clinical decision-making and uptake of neurorehabilitation technology," *J. Neuroeng. Rehabil.*, vol. 18, no. 1, pp. 1–12, 2021.

[14] R. A. Gopura, D. S. Bandara, K. Kiguchi, and G. K. Mann, "Developments in hardware systems of active upper-limb exoskeleton robots: A review," *Robot. Auton. Syst.*, vol. 75, pp. 203–220, 2016.

[15] E. Pezent, C. G. Rose, A. D. Deshpande, and M. K. O'Malley, "Design and characterization of the openwrist: A robotic wrist exoskeleton for coordinated hand-wrist rehabilitation," in *Proc. IEEE Int. Conf. Rehabil. Robot.*, 2017, pp. 720–725.

[16] C. A. Trombly and A. D. Scott, *Occupational therapy for Physical Dysfunction*. Philadelphia, PA, USA: Lippincott Williams & Wilkins, 1983.

[17] Z.-M. Li, L. Kuxhaus, J. A. Fisk, and T. H. Christophel, "Coupling between wrist flexion–extension and radial–ulnar deviation," *Clin. Biomech.*, vol. 20, no. 2, pp. 177–183, 2005.

[18] J. J. Crisco, W. M. Heard, R. R. Rich, D. J. Paller, and S. W. Wolfe, "The mechanical axes of the wrist are oriented obliquely to the anatomical axes," *J. Bone Joint Surgery. Amer. Vol.*, vol. 93, no. 2, p. 169, 2011.

[19] O. Mazumder, A. Rai, and A. Sinha, "Muscle synergy control during hand reach task on varying shoulder configuration," in *Proc. 42nd Annu. Int. Conf. IEEE Eng. Med. Biol. Soc.*, 2020, pp. 4839–4843.

[20] A.-M. Georgarakis, P. Wolf, and R. Riener, "Simplifying exosuits: Kinematic couplings in the upper extremity during daily living tasks," in *Proc. IEEE 16th Int. Conf. Rehabil. Robot.*, 2019, pp. 423–428.

[21] T. Bockemühl, N. F. Troje, and V. Dürr, "Inter-joint coupling and joint angle synergies of human catching movements," *Hum. Movement Sci.*, vol. 29, no. 1, pp. 73–93, 2010.

[22] Y. Zimmermann, A. Forino, R. Riener, and M. Hutter, "ANYexo: A versatile and dynamic upper-limb rehabilitation robot," *IEEE Robot. Autom. Lett.*, vol. 4, no. 4, pp. 3649–3656, Oct. 2019.

[23] B. Kim and A. D. Deshpande, "An upper-body rehabilitation exoskeleton harmony with an anatomical shoulder mechanism: Design, modeling, control, and performance evaluation," *Int. J. Robot. Res.*, vol. 36, no. 4, pp. 414–435, 2017.

[24] F. Molteni, G. Gasperini, G. Cannaviello, and E. Guanziroli, "Exoskeleton and end-effector robots for upper and lower limbs rehabilitation: Narrative review," *PM&R*, vol. 10, no. 9, pp. S174–S188, 2018.

[25] G. Wu et al., "ISB recommendation on definitions of joint coordinate systems of various joints for the reporting of human joint motion—part ii: shoulder, elbow, wrist and hand," *J. Biomech.*, vol. 38, no. 5, pp. 981–992, 2005.

[26] T. Nef, M. Guidali, and R. Riener, "ARMin III–arm therapy exoskeleton with an ergonomic shoulder actuation," *Appl. Bionics Biomech.*, vol. 6, no. 2, pp. 127–142, 2009.

[27] B. Kim and A. D. Deshpande, "Controls for the shoulder mechanism of an upper-body exoskeleton for promoting scapulohumeral rhythm," in *Proc. IEEE Int. Conf. Rehabil. Robot.*, 2015, vol. 2015-Septe, pp. 538–542.

[28] A. Otten et al., "LIMPACT:A hydraulically powered self-aligning upper limb exoskeleton," *IEEE/ASME Trans. Mechatronics*, vol. 20, no. 5, pp. 2285–2298, Oct. 2015.

[29] T. Nef, V. Klamroth-Marganska, U. Keller, and R. Riener, *Three-Dimensional Multi-Degree-of-Freedom Arm Therapy Robot (ARMin)*. Cham, Switzerland: Springer International Publishing, 2016, pp. 351–374.

[30] N. Schweighofer, C. E. Han, S. L. Wolf, M. A. Arbib, and C. J. Winstein, "A functional threshold for long-term use of hand and arm function can be determined: Predictions from a computational model and supporting data from the extremity constraint-induced therapy evaluation (excite) trial," *Phys. Ther.*, vol. 89, no. 12, pp. 1327–1336, 2009.

[31] S. Israely, G. Leisman, and E. Carmeli, "Improvement in arm and hand function after a stroke with task-oriented training," *Case Rep.*, vol. 2017, 2017, Art. no. bcr 2017219250.

[32] G. T. Thielman, C. M. Dean, and A. Gentile, "Rehabilitation of reaching after stroke: Task-related training versus progressive resistive exercise," *Arch. Phys. Med. Rehabil.*, vol. 85, no. 10, pp. 1613–1618, 2004.

[33] O. Lambercy et al., "Effects of a robot-assisted training of grasp and pronation/supination in chronic stroke: A pilot study," *J. Neuroeng. Rehabil.*, vol. 8, no. 1, pp. 1–12, 2011.

[34] M. Schrafl-Altermatt and V. Dietz, "Cooperative hand movements in post-stroke subjects: Neural reorganization," *Clin. Neuriophysiol.*, vol. 127, no. 1, pp. 748–754, 2016.
[35] S. Buccelli et al., "A gravity-compensated upper-limb exoskeleton for functional rehabilitation of the shoulder complex," *Appl. Sci.*, vol. 12, no. 7, 2022, Art. no. 3364.
[36] T. Bützer, O. Lambercy, J. Arata, and R. Gassert, "Fully wearable actuated soft exoskeleton for grasping assistance in everyday activities," *Soft Robot.*, vol. 8, no. 2, pp. 128–143, 2021.
[37] D. Marconi, A. Baldoni, Z. McKinney, M. Cempini, S. Crea, and N. Vitiello, "A novel hand exoskeleton with series elastic actuation for modulated torque transfer," *Mechatronics*, vol. 61, pp. 69–82, 2019.
[38] J. Rosen, J. C. Perry, N. Manning, S. Burns, and B. Hannaford, "The human arm kinematics and dynamics during daily activities—Toward a 7 DOF upper limb powered exoskeleton," in *Proc. Int. Conf. Adv. Robot.*, vol. 2005, 2005, pp. 532–539.
[39] S. Tanabe and A. Ito, "A three-dimensional analysis of the contributions of upper limb joint movements to horizontal racket head velocity at ball impact during tennis serving," *Sports Biomech.*, vol. 6, no. 3, pp. 418-4-33, 2007.
[40] A. Lees, M. Kemp, and F. Moura, "A biomechanical analysis of the soccer throw-in with a particular focus on the upper limb motion," in *Proc. Sci. Football V: Proc. 5th World Congr. Sports Sci. Football*, 2005, p. 92.
[41] F. Just et al., "Exoskeleton transparency: Feed-forward compensation vs. disturbance observer," *At - Automatisierungstechnik*, vol. 66, no. 12, pp. 1014–1026, 2018.
[42] Y. Zimmermann, E. B. Küçüktabak, F. Farshidian, R. Riener, and M. Hutter, "Towards dynamic transparency: Robust interaction force tracking using multi-sensory control on an arm exoskeleton," in *Proc. IEEE/RSJ Int. Conf. Intell. Robots Syst.*, 2020, pp. 7417–7424.
[43] A.-M. Georgarakis, R. Riener, and Y. Zimmermann, "Orthosis and method for stabilizing the position of the scapula, system for moving an arm and method for lifting a load," 2021, Art. no. Ep3892242a1.
[44] A.-M. Georgarakis, Y. Zimmermann, P. Wolf, M. Hutter, and R. Riener, "Supporting and stabilizing the scapulohumeral rhythm with a body- or robot-powered orthosis," *IEEE Trans. Med. Robot. Bionics*, vol. 4, no. 3, pp. 729–743, Aug. 2022.
[45] W. Chen, Z. Li, X. Cui, J. Zhang, and S. Bai, "Mechanical design and kinematic modeling of a cable-driven arm exoskeleton incorporating inaccurate human limb anthropomorphic parameters," *Sensors*, vol. 19, no. 20, 2019, Art. no. 4461.
[46] H. Vallery et al., "Compliant actuation of rehabilitation robots," *IEEE Robot. Autom. Mag.*, vol. 15, no. 3, pp. 60–69, Sep. 2008.
[47] M. Sommerhalder, Y. Zimmermann, B. Cizmeci, R. Riener, and M. Hutter, "Physical human-robot interaction with real active surfaces using haptic rendering on point clouds," in *Proc. IEEE/RSJ Int. Conf. Intell. Robots Syst.*, 2020, pp. 9767–9773.
[48] C. P. Neu, J. J. Crisco, and S. W. Wolfe, "In vivo kinematic behavior of the radio-capitate joint during wrist flexion–extension and radio-ulnar deviation," *J. Biomech.*, vol. 34, no. 11, pp. 1429–1438, 2001.
[49] U. Keller, H. J. Van Hedel, V. Klamroth-Marganska, and R. Riener, "ChARMin: The first actuated exoskeleton robot for pediatric arm rehabilitation," *IEEE/ASME Trans. Mechatronics*, vol. 21, no. 5, pp. 2201–2213, Oct. 2016.
[50] J. C. Perry, J. Rosen, and S. Burns, "Upper-limb powered exoskeleton design," *IEEE/ASME Trans. Mechatronics*, vol. 12, no. 4, pp. 408–417, Aug. 2007.
[51] T. L. Brooks, "Telerobotic response requirements," in *Proc. IEEE Conf. Syst., Man Cybern.*, 1990, pp. 113–120.
[52] D. H. Gates, L. S. Walters, J. Cowley, J. M. Wilken, and L. Resnik, "Range of motion requirements for upper-limb activities of daily living," *Amer. J. Occup. Ther.*, vol. 70, no. 1, pp. 7001350010p1–7001350010p10, 2016.
[53] R. M. Paine and M. Voight, "The role of the scapula," *Int. J. Sports Phys. Ther.*, vol. 8, no. 5, pp. 617–629, 2013.
[54] V. T. Inman, J. B. Saunders, and L. C. Abbott, "Observations on the function of the shoulder joint," *J. Bone Joint Surg.*, vol. 26, no. 1, pp. 1–30, 1944.
[55] C. Dario Bellicoso, C. Gehring, J. Hwangbo, P. Fankhauser, and M. Hutter, "Perception-less terrain adaptation through whole body control and hierarchical optimization," in *Proc. IEEE-RAS Int. Conf. Humanoid Robots*, 2016, pp. 558–564.
[56] A. H. Stienen and A. Q. Keemink, "Visualization of shoulder range of motion for clinical diagnostics and device development," in *Proc. IEEE Int. Conf. Rehabil. Robot.*, 2015, vol. 2015, pp. 816–821.
[57] D. C. Boone and S. P. Azen, "Normal range of motion of joints in male subjects," *J. Bone Joint Surgery. Amer.*, vol. 61, no. 5, pp. 756–759, 1979.
[58] S. Namdari et al., "Defining functional shoulder range of motion for activities of daily living," *J. Shoulder Elbow Surg.*, vol. 21, no. 9, pp. 1177–1183, 2012.
[59] J.-Y. Hogrel et al., "Development of a french isometric strength normative database for adults using quantitative muscle testing," *Arch. Phys. Med. Rehabil.*, vol. 88, no. 10, pp. 1289–1297, 2007.
[60] K. Plewa, J. R. Potvin, and J. P. Dickey, "Wrist rotations about one or two axes affect maximum wrist strength," *Appl. Ergonom.*, vol. 53, pp. 152–160, 2016.
[61] J. Y. Hogrel et al., "Development of a french isometric strength normative database for adults using quantitative muscle testing," *Arch. Phys. Med. Rehabil.*, vol. 88, no. 10, pp. 1289–1297, 2007.
[62] J. Aizawa et al., "Ranges of active joint motion for the shoulder, elbow, and wrist in healthy adults," *Disabil. Rehabil.*, vol. 35, no. 16, pp. 1342–9, 2013.
[63] D. J. Magermans, E. K. J. Chadwick, H. E. J. Veeger, and F. C. T. Van Der Helm, "Requirements for upper extremity motions during activities of daily living," *Clin. Biomech.*, vol. 20, no. 6, pp. 591–599, 2005.
[64] G. S. Fleisig, R. F. Escamilla, J. R. Andrews, T. Matsuo, Y. Satterwhite, and S. W. Barrentine, "Kinematic and kinetic comparison between baseball pitching and football passing," *J. Appl. Biomech.*, vol. 12, no. 2, pp. 207–224, 1996.
[65] F. C. Hagerman, R. Lawrence, and M. C. Mansfield, "A comparison of energy expenditure during rowing and cycling ergometry," *Med. Sci. Sports Exercise*, vol. 20, no. 5, pp. 479–488, 1988.